

The variance of identity-by-descent sharing in the Wright-Fisher model

Shai Carmi,¹ Pier Francesco Palamara,¹ Vladimir Vacic,¹ Todd Lencz,² Ariel Darvasi,³ and Itsik Pe'er^{1,4}

¹Department of Computer Science, Columbia University, New York, NY 10025, USA

²Department of Psychiatry, Division of Research,

The Zucker Hillside Hospital Division of the North Shore-Long Island Jewish Health System, Glen Oaks, NY, 11004, USA

³Department of Genetics, The Institute of Life Sciences,

The Hebrew University of Jerusalem, Givat Ram, Jerusalem, 91904, Israel

⁴Center for Computational Biology and Bioinformatics,

Columbia University, New York, NY, 10032, USA

(Dated: December 19, 2012)

Widespread sharing of long, identical-by-descent (IBD) genetic segments is a hallmark of populations that have experienced recent genetic drift. Detection of these IBD segments has recently become feasible, enabling a wide range of applications from phasing and imputation to demographic inference. Here, we study the distribution of IBD sharing in the Wright-Fisher model. Specifically, using coalescent theory, we calculate the variance of the total sharing between random pairs of individuals. We then investigate the cohort-averaged sharing: the average total sharing between one individual and the rest of the cohort. We find that for large cohorts, the cohort-averaged sharing is distributed approximately normally and surprisingly, the variance of this distribution does not vanish large even for large cohorts, implying the existence of “hyper-sharing” individuals. The presence of such individuals has consequences for the design of sequencing studies, since, if they are selected for whole-genome sequencing, a larger fraction of the cohort can be subsequently imputed. We calculate the expected gain in power of imputation by IBD, and subsequently, in power to detect an association, when individuals are either randomly selected or are specifically chosen to be the hyper-sharing individuals. Using our framework, we also compute the variance of an estimator of the population size that is based on the mean IBD sharing and the variance in the sharing between inbred siblings. Finally, we study IBD sharing in an admixture pulse model, and show that in the Ashkenazi Jewish population the admixture fraction is correlated with the cohort-averaged sharing.

I. INTRODUCTION

In isolated populations, even purported unrelated individuals often share genetic material that is *identical-by-descent*, or IBD. Traditionally, the term IBD sharing referred to co-ancestry at a single site (or autozygosity, in the case of a diploid individual) and was widely investigated as a measure of the degree of inbreeding in a population [1]. Recent years have brought dramatic increases in the quantity and density of available genetic data, and together with new computational tools, enabled the detection of IBD sharing of entire genomic segments (see, e.g., [2–8]). The availability of IBD detection tools that are efficient enough to detect shared segments in large cohorts has resulted in numerous applications, from demographic inference [9, 10] and characterization of populations [11] to selection detection [12], relatedness detection and pedigree reconstruction [13–16], prioritization of individuals for sequencing [17], inference of HLA type [18], detection of haplotypes associated with a disease or a trait [19–21], imputation [22], and phasing [23].

Recently, some of us used coalescent theory to calculate several theoretical quantities of IBD sharing under a number of demographic histories. Then, shared segments were detected in real populations, and their demographic histories were inferred [10]. Here, we expand upon [10] to investigate additional aspects of the stochastic variation in IBD sharing. Specifically, we provide a precise calculation for the variance of the total sharing in the

Wright-Fisher model, either between a random pair of individuals or between one individual and all others in the cohort.

Understanding the variation in IBD sharing is an important theoretical characterization of the Wright-Fisher model, and additionally, it has several practical applications. For example, it can be used to calculate the variance of an estimator of the population size that is based on the sharing between random pairs. In a different domain, the variance in IBD sharing is needed to accurately assess strategies for sequencing studies, specifically, in prioritization of individuals to be sequenced. This is because imputation strategies use IBD sharing between sequenced individuals and genotyped, not-sequenced individuals to increase the number of effective sequences analyzed in the association study [17, 22, 23].

In the remainder of the paper, we first review the derivation of the mean fraction of the genome shared between two individuals [10]. We then calculate the variance of this quantity using coalescent theory with recombination. We provide a number of approximations, one of which results in a surprisingly simple expression, which is then generalized to a variable population size and to the sharing of segments in a length range. We also numerically investigate the pairwise sharing distribution and provide an approximate fit. We then turn to the average total sharing between each individual and the entire cohort. We show that this quantity, which we term the cohort-averaged sharing, is approximately normally distributed, but is much wider than naively expected,

implying the existence of hyper-sharing individuals. We consider several applications: the number of individuals needed to be sequenced to achieve a certain imputation power and the implications to disease mapping, inference of the population size based on the total sharing, and the variance of the sharing between siblings. We finally calculate the mean and the variance of the sharing in an admixture pulse model and show numerically that admixture results in a broader than expected cohort-averaged sharing. Therefore, large variance of the cohort-averaged sharing can indicate admixture. In the Ashkenazi Jewish population, we show that the cohort-averaged sharing is strongly anti-correlated with the fraction of European ancestry.

II. RESULTS

A. Variation in IBD sharing in the Wright-Fisher model

1. Definitions

The Wright-Fisher model.— We consider the standard Wright-Fisher model for a finite, isolated population, described by $2N$ haploid chromosomes, where each pair of chromosomes corresponds to one diploid individual. Each chromosome in the current generation descends, with equal probability, from one of the chromosomes in the previous generation (generations are non-overlapping), and recombination occurs at rate $0.01/\text{cM}$ per generation. The Wright-Fisher model has been widely investigated both in forward dynamics and under the coalescent [24]. For simplicity of notation, we denote the number of individuals, or the population size, as N , even though we really refer to the number of haploids and not the number of individuals. Throughout most of the analysis, we assume that each individual carries a single chromosome of length L centiMorgans (cM).

IBD sharing.— We say that a genomic segment is shared, or is IBD, between two individuals if it is longer than $m(\text{cM})$ and it has been inherited without recombination from a single common ancestor. We do not require the shared segments to be completely identical. That is, if any mutation has occurred since the time of the most recent common ancestor (MRCA), that would not disqualify the segments from being shared IBD according to our definition. The reason is that even in the presence of mutations, an order of magnitude calculation shows that regardless of the segment length, two individuals sharing a segment are expected to differ in just ≈ 1 site along the segment (see the Supplementary Material, Section S1.1). Therefore, in a long IBD segment, the number of differences should be very small compared to the number of matches. In practice, there are also other sources of error in IBD detection, most notably phase switch errors. We assume, however, that there always exists a large enough length threshold above which segments

are detectable without errors [3, 7], which corresponds to the parameter m introduced above; the precise value of the threshold will depend on the genotyping/sequencing technology. We assume that information is available for M markers, uniformly distributed (in genetic distance) along the chromosome, and densely enough that any effect caused by the discreteness of the markers is negligible (say, if $m \cdot (M/L) \gg 1$). We define the *total sharing* between two individuals as the fraction of their markers that are found in shared segments.

2. Mean total sharing

In this subsection, we review the derivation of the mean fraction of the genome found in segments shared between two individuals [10]. We assume that the coalescent process along the chromosome can be approximated by the Sequentially Markov Coalescent [25], and ignore the different behavior of sites at the ends of the chromosome. Consider first a single site s and assume that its MRCA dates g generations ago. The total length ℓ of the segment in which the site is found is the sum of ℓ_R and ℓ_L , where ℓ_R and ℓ_L are the segment lengths to the right and left of s , respectively (all lengths are in cM). The distributions of ℓ_R and ℓ_L are exponential with rate $g/50$, since the two individuals were separated by $2g$ meioses, each of which introduces a recombination event with rate $0.01/\text{cM}$, and the nearest recombination would terminate the shared segment. The probability π of the total segment length, ℓ , to exceed m is, given g ,

$$\pi|g = \int_m^\infty \ell \left(\frac{g}{50}\right)^2 e^{-\frac{g}{50}\ell} d\ell = \left(1 + \frac{mg}{50}\right) e^{-\frac{mg}{50}}. \quad (1)$$

According to coalescent theory in the Wright-Fisher model, under the continuous-time scaling $g \rightarrow Nt$ the times to the MRCA are exponentially distributed with rate 1: $\Phi(t) = e^{-t}$. Therefore,

$$\begin{aligned} \pi &= \int_0^\infty e^{-t} \left(1 + \frac{mNt}{50}\right) e^{-\frac{mNt}{50}} dt \\ &= \frac{100(25 + mN)}{(50 + mN)^2}. \end{aligned} \quad (2)$$

The total fraction of the genome found in shared segments is

$$f_T = \frac{1}{M} \sum_{s=1}^M I(s), \quad (3)$$

where $I(s)$ is the indicator that site s is in a shared segment, and the sum is over all sites. The mean fraction of genome shared is

$$\langle f_T \rangle = \frac{1}{M} \sum_{s=1}^M \langle I(s) \rangle = \pi = \frac{100(25 + mN)}{(50 + mN)^2}, \quad (4)$$

where $\langle \cdot \rangle$ denotes the average over all ancestral processes. As expected, for $mN \rightarrow \infty$, $\langle f_T \rangle \rightarrow 0$ and for $mN \rightarrow 0$, $\langle f_T \rangle \rightarrow 1$. For large N , we have $\langle f_T \rangle \approx 100/(mN)$.

3. The variance of the total sharing

We now turn to calculate the variance of the total sharing. Using Eq. (3),

$$\begin{aligned}\text{Var}[f_T] &= \text{Var}\left[\frac{1}{M}\sum_{s=1}^M I(s)\right] \\ &= \frac{\pi(1-\pi)}{M} + \frac{1}{M^2}\sum_{s_1}\sum_{s_2 \neq s_1} \text{Cov}[I(s_1), I(s_2)] \\ &= \frac{\pi(1-\pi)}{M} + \frac{1}{M^2}\sum_{s_1}\sum_{s_2 \neq s_1} [\pi_2(s_1, s_2) - \pi^2],\end{aligned}$$

where $\pi_2(s_1, s_2)$ is the probability that both markers s_1 and s_2 are on shared segments and π is given by Eq. (2). In the rest of the section, we assume that each individual carries one chromosome only, for if we have c chromosomes, each of length L_i , then (if the two individuals are not close relatives)

$$f_T = \frac{\sum_{i=1}^c L_i f_{T,(i)}}{\sum_{i=1}^c L_i},$$

and the variance is

$$\text{Var}[f_T] = \frac{\sum_{i=1}^c L_i^2 \text{Var}[f_{T,(i)}]}{(\sum_{i=1}^c L_i)^2}, \quad (5)$$

where $f_{T,(i)}$ is the total sharing in chromosome i , assumed independent of the other chromosomes. Rewriting $\pi_2(s_1, s_2)$ as $\pi_2(k)$, where k is the number of markers separating s_1 and s_2 , we have

$$\text{Var}[f_T] = \frac{\pi(1-\pi)}{M} + \frac{2}{M^2}\sum_{k=1}^M (M-k) [\pi_2(k) - \pi^2]. \quad (6)$$

All is left is evaluate $\pi_2(k)$, for which we provide three approximations. The first is presented below and the second (which is a variation of the first) is presented in Supplementary Section S1.3. The third approximation, which is the most crude but which yields an explicit dependence on the population parameters, is presented in Section II A 4.

In the first approach, we assume that once the times t_1, t_2 to the MRCA at the two sites are known, the sites are (or are not) in shared segments independently of each other, and with probabilities given by Eq. (1). Clearly, this assumption is violated when both sites belong to the same shared segment, and in Supplementary Section S1.3, we show how this assumption can be avoided (but in the cost of significantly complicating the analysis). Nevertheless, it gives a good approximation, as we will later

see (Figure 2). We can therefore use Eq. (1) to write

$$\begin{aligned}\pi_2(k) &\approx \int_0^\infty \int_0^\infty dt_1 dt_2 \Phi(t_1, t_2) \times \\ &\times \left(1 + \frac{mNt_1}{50}\right) e^{-\frac{mNt_1}{50}} \left(1 + \frac{mNt_2}{50}\right) e^{-\frac{mNt_2}{50}} \\ &= \hat{\Phi}\left(\frac{mN}{50}, \frac{mN}{50}\right) - m \frac{\partial}{\partial m} \hat{\Phi}\left(\frac{mN}{50}, \frac{mN}{50}\right) \\ &+ m^2 \left[\frac{\partial}{\partial m_1} \frac{\partial}{\partial m_2} \hat{\Phi}\left(\frac{m_1 N}{50}, \frac{m_2 N}{50}\right) \right]_{\substack{m_1=m \\ m_2=m}},\end{aligned} \quad (7)$$

where $\Phi(t_1, t_2)$ is the joint PDF of t_1 and t_2 and

$$\hat{\Phi}(q_1, q_2) = \int_0^\infty \int_0^\infty e^{-q_1 t_1 - q_2 t_2} \Phi(t_1, t_2) dt_1 dt_2$$

is the Laplace transform of $\Phi(t_1, t_2)$. We therefore reduced the problem of finding $\pi_2(k)$ into that of finding $\hat{\Phi}(q_1, q_2)$.

To find $\Phi(t_1, t_2)$ (or rather, its Laplace transform), we use the continuous-time Markov chain representation of the coalescent with recombination [24, 26, 27]. The chain is illustrated in Figure 1. Initially (present time), the chain is in state 1, corresponding to two chromosomes carrying two sites each. The chain terminates at state 8, when both sites have reached their MRCA. To construct the chain, coalescence events were assumed to occur at rate 1 and recombination events at rate $\rho/2$, where $\rho = 2N \frac{k}{M} L/100$ is the scaled recombination rate [24].

Denote by $P_i(t)$ the probability that the chain is at state i at time t , given that it started at state 1. The probability that the two sites have reached their MRCA simultaneously in the time range $[t, t+dt]$ is $P_1(t)dt$, since this is the product of the probability that the chain is at state 1 at time t ($P_1(t)$) and the probability of the transition $1 \rightarrow 8$ in the given time interval (dt). The probability that only the left site has reached its MRCA (and the right site has not) in $[t, t+dt]$ is $P_2(t)dt + P_3(t)dt$: this corresponds to the transitions $2 \rightarrow 5$ and $3 \rightarrow 7$. This is also the probability that only the right side has reached its MRCA in $[t, t+dt]$ (transitions $2 \rightarrow 4$, $3 \rightarrow 6$). Finally, the probability that the left site has reached its MRCA in $[t_1, t_1+dt_1]$ and that the right side has reached its MRCA in $[t_2, t_2+dt_2]$ ($t_2 > t_1$) is $[P_2(t_1) + P_3(t_1)]dt_1 e^{-(t_2-t_1)}dt_2$. This is true, because the exit rate from state 5 and 7 is 1; therefore, the probability that the chain will wait at one of those states for time $(t_2 - t_1)$ and then leave to the terminal state is $e^{-(t_2-t_1)}dt_2$. Similar considerations apply for the case $t_1 > t_2$ (with the transitions $2 \rightarrow 4$ and $3 \rightarrow 6$). In sum, for $t_1, t_2 > 0$,

$$\begin{aligned}\Phi(t_1, t_2) &= P_1(t_1)\delta(t_2 - t_1) \\ &+ [P_2(t_1) + P_3(t_1)]e^{-(t_2-t_1)}\Theta(t_2 - t_1) \\ &+ [P_2(t_2) + P_3(t_2)]e^{-(t_1-t_2)}\Theta(t_1 - t_2),\end{aligned}$$

where $\delta(t)$ is the Dirac delta function and $\Theta(t) = 1$ for $t > 0$ and is otherwise zero. Laplace transforming the

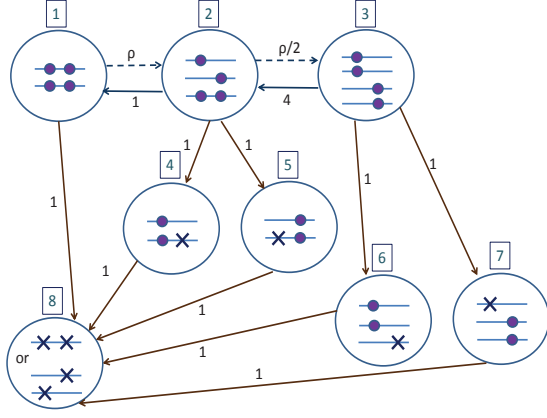


FIG. 1: **An illustration of the continuous-time Markov chain representation of the coalescent with recombination** [24, 27]. Circles correspond to states, with the state number in a box on top of each circle. Arrows connecting circles represent transitions (solid lines: coalescence events; dashed lines: recombination events), with their rates indicated. The lines inside each circle represent chromosomes with two sites each. Ancestral sites are indicated as either small circles (as long as there are still two lineages carrying the ancestral material) or crosses (whenever the two lineages coalesced and the site has reached its MRCA). Transitions leading to the MRCA in one or two sites are colored brown. Transitions between states 4 and 6 and between 5 and 7 are not indicated, as they do not affect the final coalescence times. The schematic was adapted from [24].

last equation,

$$\begin{aligned}
 \widehat{\Phi}(q_1, q_2) &= \int_0^\infty \int_0^\infty e^{-q_1 t_1 - q_2 t_2} P_1(t_1) \delta(t_2 - t_1) dt_1 dt_2 \\
 &+ \int_0^\infty \int_{t_1}^\infty e^{-q_1 t_1 - q_2 t_2} [P_2(t_1) + P_3(t_1)] e^{-(t_2 - t_1)} dt_2 dt_1 \\
 &+ \int_0^\infty \int_{t_2}^\infty e^{-q_1 t_1 - q_2 t_2} [P_2(t_2) + P_3(t_2)] e^{-(t_1 - t_2)} dt_1 dt_2 \\
 &= \widehat{P}_1(q_1 + q_2) \\
 &+ \frac{1}{q_2 + 1} \int_0^\infty e^{-(q_1 + q_2) t_1} [P_2(t_1) + P_3(t_1)] dt_1 \\
 &+ \frac{1}{q_1 + 1} \int_0^\infty e^{-(q_1 + q_2) t_2} [P_2(t_2) + P_3(t_2)] dt_2 \\
 &= \widehat{P}_1(q_1 + q_2) \\
 &+ [\widehat{P}_2(q_1 + q_2) + \widehat{P}_3(q_1 + q_2)] \left[\frac{1}{q_1 + 1} + \frac{1}{q_2 + 1} \right]. \quad (8)
 \end{aligned}$$

In the last equation, $\widehat{P}_i(q) = \int_0^\infty e^{-qt} P_i(t) dt$ ($i = 1, 2, 3$) are the Laplace transforms of $P_i(t)$. The Laplace transforms can be calculated using the general relation [28]

$$\widehat{P}_i(q) = (qI - Q)^{-1}_{ii}, \quad (9)$$

where Q is the transition rate matrix: Q_{ij} is the transi-

tion rate from i to $j \neq i$ and $Q_{ii} = -\sum_{j \neq i} Q_{ij}$,

$$Q = \begin{pmatrix} -1 - \rho & \rho & 0 & 0 & 0 & 0 & 0 & 1 \\ 1 & -3 - \rho/2 & \rho/2 & 1 & 1 & 0 & 0 & 0 \\ 0 & 4 & -6 & 0 & 0 & 1 & 1 & 0 \\ 0 & 0 & 0 & -1 & 0 & 0 & 0 & 1 \\ 0 & 0 & 0 & 0 & -1 & 0 & 0 & 1 \\ 0 & 0 & 0 & 0 & 0 & -1 & 0 & 1 \\ 0 & 0 & 0 & 0 & 0 & 0 & -1 & 1 \\ 0 & 0 & 0 & 0 & 0 & 0 & 0 & 0 \end{pmatrix}. \quad (10)$$

Using Eqs. (8), (9), and (10), and MATHEMATICA,

$$\widehat{\Phi}(q_1, q_2) = \frac{2AB + C(D + q_1 q_2) + E}{A[2(A - q_1 q_2)B + CD + E]}, \quad (11)$$

where $A = (1 + q_1)(1 + q_2)$, $B = (3 + q_1 + q_2)(6 + q_1 + q_2)$, $C = \rho(2 + q_1 + q_2)$, $D = 13 + 3(q_1 + q_2)$ and $E = \rho^2(2 + q_1 + q_2)$. Eq. (11) was also derived in [29], using the birth-and-death-process description of the coalescent with recombination, and can also be derived using the Feynman-Kac formula (see Supplementary Section S1.4). Substituting, using MATHEMATICA, Eq. (11) in (7) and then in (6) gives an expression for the variance,

$$\text{Var}[f_T] = \mathcal{F}(N, m, L, M). \quad (12)$$

The function \mathcal{F} is too long to reproduce here, but can be found in the Supplementary MATLAB code (File S2). For further discussion on the approximations made, see Supplementary Section S1.2. The *standard deviation* (SD) of the total sharing is defined as usual as $\sigma_{f_T} \equiv \sqrt{\text{Var}[f_T]}$.

To evaluate the accuracy of our expressions for the mean and SD of the total sharing, we used the GENOME coalescent simulator [30], along with an add-on that returns, for each generated genealogy, the locations of the segments that are IBD between each pair of individuals [10]. The simulation results (see also Methods) are presented and compared to the theory in Figure 2. In each panel, we varied one of N , m , and L , keeping the two others fixed (as long as the marker density is large enough, the number of markers M has no effect on the variance). Across most of the parameter space, our expressions agree well with simulations. Notable deviations, however, arise for the SD in particularly short or long chromosomes. For these cases, the second, more complicated approximation, which we mentioned above and appears in Supplementary Section S1.3, is more accurate (Figure 2).

4. An approximate explicit expression

In this subsection, we derive another, simpler approximation of the variance, one that is less accurate but that has an explicit dependence on the population and genetic parameters. The gist of this approximation is that the main contribution to the variance comes from the long-distance probability of pairs of sites to reside on the same

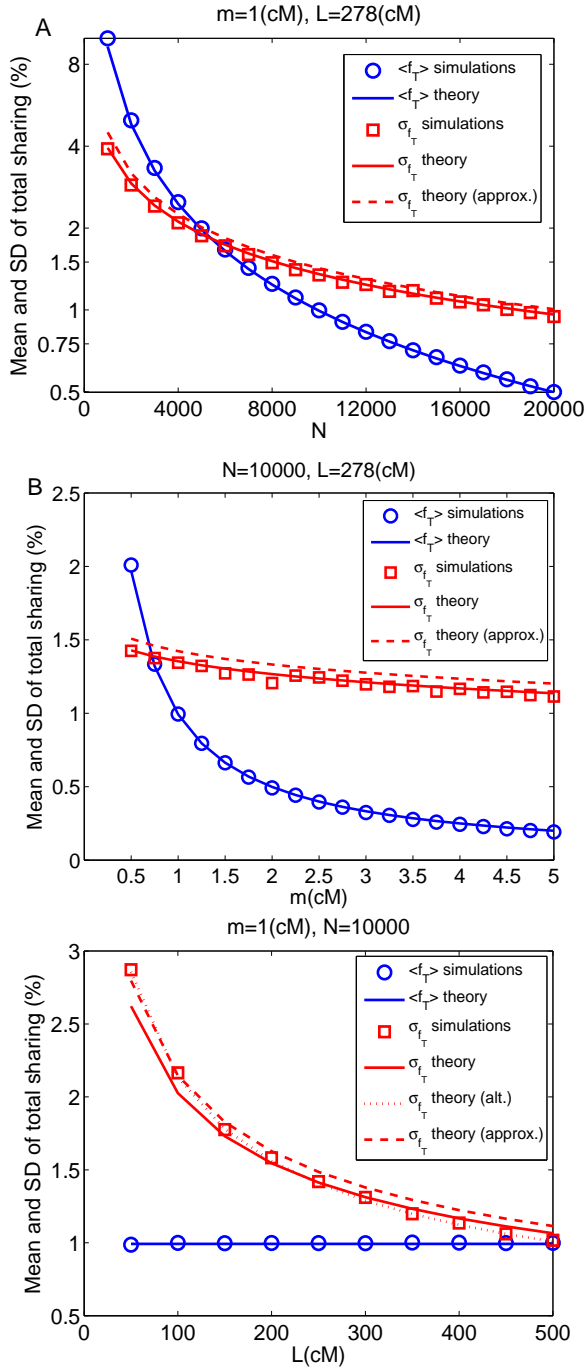


FIG. 2: The mean and standard deviation of the total sharing. For each parameter set, we used the GENOME coalescent simulator to generate a number of genealogies (from a population of size N and for one chromosome of size L), and then calculated the lengths of IBD shared segments between random individuals. Each panel presents the results for the mean and standard deviation (SD) of the total sharing, that is, for each pair, the total fraction (in percentages) of the genome that is found in shared segments of length $\geq m$. Simulation results are represented by symbols, and theoretical results by lines (Eq. (4) for the mean and Eq. (12) for the SD are plotted in solid lines; the approximate form for the SD, Eq. (15), is shown in dashed lines). **A** We fixed $m = 1\text{cM}$ and $L = 278\text{cM}$ (the size of the human chromosome 1 [31]), and varied N . **B** Same as A, but with fixed $N = 10000$ and varying m . **C** Fixed N and m and varying chromosome length L . In this panel, we also plotted the result of an alternative, more elaborate calculation of the variance (dotted line; see Supplementary Section S1.3).

segment. Denote the distance between two given sites by d , and assume that $d > m$. For a given pair of individuals, if there was no recombination event between the two sites in the history of the two lineages, then both sites lie on a shared segment of length $\geq d > m$. Of course, even if there was a recombination event, the two sites could still be each on a different shared segment. However, this occurs with probability very close to π^2 , the probability that the two sites are on shared segments given that they are independent.

In terms of Eq. (6), the above approximation translates to

$$\pi_2(k) - \pi^2 \approx p_{\text{nr}}, \quad (13)$$

where p_{nr} is the probability of no recombination,

$$p_{\text{nr}} = \frac{1}{1 + \rho} = \frac{1}{1 + Nd/50} \approx \frac{50}{Nd} \quad (14)$$

for distant sites where $Nd \gg 50$. This is true because in the ancestral process (Figure 1), no recombination corresponds to a coalescence event taking place before any recombination event. Since the coalescence rate is 1 and the recombination rate is ρ , Eq. (14) follows. We can then further simplify and neglect the contribution to the variance from sites separated by short distance $d < m$. Finally, we can also neglect the single-site term of the variance, since it scales as $1/M$ and therefore vanishes when the markers are dense. Overall, the simplified Eq. (6) gives

$$\begin{aligned} \text{Var}[f_T] &\approx \frac{2}{M^2} \sum_{k=m}^M (M-k) \frac{50}{Nk \frac{L}{M}} \\ &\approx \frac{100}{MNL} \int_{m \frac{M}{L}}^M \frac{M-k}{k} dk = \frac{100}{NL} \int_{m/L}^1 \frac{1-x}{x} dx \\ &= \frac{100}{NL} \left[\ln\left(\frac{L}{m}\right) - 1 + \frac{m}{L} \right] \approx \frac{100}{NL} \ln\left(\frac{L}{m}\right) \end{aligned} \quad (15)$$

for $L \gg m$. Nicely, Eq. (15) provides an explicit (and rather simple) dependence on N , L and m , and as expected, the expression does not depend on the marker density. Eq. (15) is also plotted in Figure 2, showing that it fits quite well to the simulation results, although it is usually less accurate than Eq. (12).

For the entire (autosomal) human genome, we use Eq. (5),

$$\text{Var}[f_T] = \frac{100 \sum_{i=1}^{22} L_i \ln\left(\frac{L_i}{m}\right)}{N \left(\sum_{i=1}^{22} L_i\right)^2}.$$

For $m \approx 1\text{cM}$, the last equation gives

$$\sigma_{f_T} \approx \frac{0.382}{\sqrt{N}}. \quad (16)$$

A variable population size.— The framework presented above can be extended to calculate the variance for a

generalization of the Wright-Fisher model in which the population size is allowed to change in time. Denote the population size as $N(t) = N_0\lambda(t)$, where t is the time (scaled by N_0) before present. The PDF of the (scaled) coalescence time for two lineages is (see, e.g., [32])

$$\Phi(t) = \frac{e^{-\int_0^t \frac{dt'}{\lambda(t')}}}{\lambda(t)}.$$

As shown in [10], the mean of the total sharing is obtained by substituting the above $\Phi(t)$ in Eq. (2), giving

$$\langle f_T \rangle = \int_0^\infty \Phi(t) \left(1 + \frac{mN_0t}{50}\right) e^{-\frac{mN_0t}{50}} dt. \quad (17)$$

For the variance, following Eq. (13), we need to calculate the probability of no recombination, p_{nr} . For sites distance d apart,

$$p_{\text{nr}} = \int_0^\infty \Phi(t) e^{-\frac{tN_0d}{50}} dt, \quad (18)$$

since for coalescence time t the sites are separated by $2N_0t$ meioses, in each of which the probability of no recombination is $e^{-d/100}$. Eq. (18) reduces to Eq. (14) for $\lambda(t) = 1$ (where $\Phi(t) = e^{-t}$). Eq. (18) can then be substituted into Eq. (15), giving

$$\begin{aligned} \text{Var}[f_T] &\approx \frac{2}{M^2} \sum_{k=\frac{M}{L}}^M (M-k) \int_0^\infty \Phi(t) e^{-tN_0k\frac{L}{M}/50} dt \\ &\approx 2 \int_{m/L}^1 (1-x) \left[\int_0^\infty \Phi(t) e^{-txN_0L/50} dt \right] dx. \end{aligned} \quad (19)$$

In Supplementary Section S1.5, we work out an example of a linearly expanding population, where Eq. (18) was solvable and the integral of Eq. (19) was evaluated numerically.

The total sharing in a length range.— Consider the quantity $f_{T;\ell_1,\ell_2}$, defined as the total fraction of the genome found in shared segments of length in the range $[\ell_1, \ell_2]$. Clearly, $f_{T;\ell_1,\ell_2} = f_{T;m=\ell_1} - f_{T;m=\ell_2}$, that is, the difference between the usual total sharing when $m = \ell_1$ and when $m = \ell_2$. The average is simply $\langle f_{T;\ell_1,\ell_2} \rangle = \langle f_{T;m=\ell_1} \rangle - \langle f_{T;m=\ell_2} \rangle = \frac{100N^2(\ell_2-\ell_1)[25(\ell_1+\ell_2)+\ell_1\ell_2N]}{(50+\ell_1)^2(50+\ell_2)^2}$, an equation that was derived in [10] and then used for demographic inference. Here, we calculate the variance, $\text{Var}[f_{T;\ell_1,\ell_2}]$, as follows,

$$\begin{aligned} \text{Var}[f_{T;\ell_1,\ell_2}] &= \text{Var}[f_{T;m=\ell_1} - f_{T;m=\ell_2}] \\ &= \text{Var}[f_{T;m=\ell_1}] + \text{Var}[f_{T;m=\ell_2}] - 2\text{Cov}[f_{T;m=\ell_1}, f_{T;m=\ell_2}]. \end{aligned} \quad (20)$$

The covariance term can be expanded as

$$\begin{aligned} \text{Cov} \left[\frac{1}{M} \sum_{s_1=1}^M I(s_1; m = \ell_1), \frac{1}{M} \sum_{s_2=1}^M I(s_2; m = \ell_2) \right] \\ = \frac{1}{M^2} \sum_{s_1} \sum_{s_2} \text{Cov}[I(s_1; m = \ell_1), I(s_2; m = \ell_2)] \\ = \frac{1}{M^2} \sum_{s_1} \sum_{s_2} [\pi_2(s_1, \ell_1; s_2, \ell_2) - \pi_{m=\ell_1} \pi_{m=\ell_2}], \end{aligned}$$

where $I(s; m = \ell)$ is the indicator that site s is in a shared segment of length at least ℓ , $\pi_{m=\ell}$ is the probability associated with the indicator, and $\pi_2(s_1, \ell_1; s_2, \ell_2)$ is the probability that site s_1 is in a shared segment of length at least ℓ_1 and site s_2 is in a shared segment of length at least ℓ_2 . The key approximation, similar to the one made in subsection II A 4 (Eq. (15)), is that $\pi_2(s_1, \ell_1; s_2, \ell_2) - \pi_{m=\ell_1} \pi_{m=\ell_2}$ is non-zero only when the two sites lie on the same segment, and that the segment is *longer than* ℓ_2 . Defining p_{nr} , as before, as the probability of no recombination between s_1 and s_2 in the history of the two individuals, we have

$$\begin{aligned} \text{Cov}[f_{T;m=\ell_1}, f_{T;m=\ell_2}] &\approx \frac{2}{M^2} \sum_{k=\ell_2}^M (M-k) p_{\text{nr}}(k) \\ &\approx \text{Var}[f_{T;m=\ell_2}], \end{aligned} \quad (21)$$

where the last step follows from Eq. (15). Substituting Eq. (21) into Eq. (20), we obtain

$$\text{Var}[f_{T;\ell_1,\ell_2}] \approx \text{Var}[f_{T;m=\ell_1}] - \text{Var}[f_{T;m=\ell_2}].$$

For a constant population size, using Eq. (15) (taking all terms in that equation) gives

$$\text{Var}[f_{T;\ell_1,\ell_2}] \approx \frac{100}{NL} \left[\ln \left(\frac{\ell_2}{\ell_1} \right) - \frac{\ell_2 - \ell_1}{L} \right]. \quad (22)$$

Eq. (22) is compared to simulations in Figure 3, showing good agreement. Note that as long as $\ell_1, \ell_2 \ll L$, the variance depends only on the ratio ℓ_2/ℓ_1 .

5. The total sharing distribution and an error model

Having the first two moments of the total sharing, we sought to find its distribution, $P(f_T)$. While we could not find an exact expression, we could find, inspired by the numerical results of [13], a reasonable fit. Huff et al. [13] showed empirically that for HapMap's Europeans [31], the number of shared segments between random individuals was distributed as a Poisson, and that the length of each segment was distributed exponentially with a lower cutoff at m , independent of the number of segments. If this is true also for the Wright-Fisher model, then the total length of the shared segments, defined as $L_T = L f_T$,

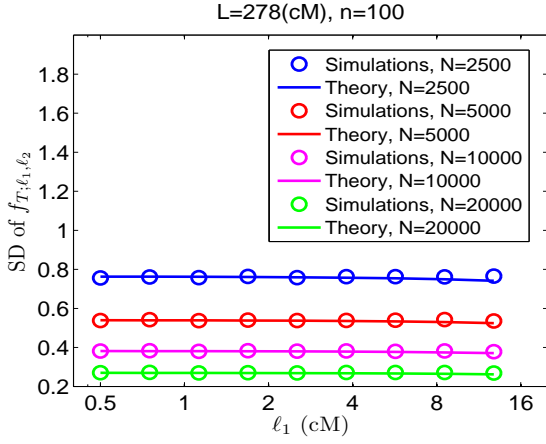


FIG. 3: **The standard deviation (SD) of the total sharing in a length range.** Simulation results (symbols) are shown for the SD of the fraction of the genome found in shared segments of specific length ranges. The total sharing for each range was calculated for random pairs of individuals in Wright-Fisher populations of the sizes indicated in the legend. The SD is plotted vs. the starting point of each length range, ℓ_1 (where for each ℓ_1 , the successive data point is ℓ_2). Note the logarithmic scale in the x-axis and hence that ℓ_2/ℓ_1 is fixed (equal to 1.5). Theory (lines) corresponds to Eq. (22).

is distributed as a sum of a Poisson distributed number of these exponentials. In equations,

$$P(L_T) = \sum_{n=0}^{\infty} e^{-n_0} \frac{n_0^n}{n!} \cdot \text{Prob}\{\ell_1 + \ell_2 + \dots + \ell_n = L_T\}, \quad (23)$$

where n_0 is the mean number of segments, the density of the ℓ_i s is $\exp[-(\ell_i - m)/\ell_0]/\ell_0$ ($\ell_0 + m$ is the mean segment length), and $\ell_i \geq m$. Such an expression is easier to handle in Laplace space, where the Laplace transform of $P(L_T)$, $\tilde{P}(s)$, is

$$\begin{aligned} \tilde{P}(s) &= \sum_{n=0}^{\infty} e^{-n_0} \frac{n_0^n}{n!} \frac{e^{-mns}}{[s\ell_0 + 1]^n} \\ &= \exp \left[-n_0 \left(1 - \frac{e^{-ms}}{s\ell_0 + 1} \right) \right], \end{aligned} \quad (24)$$

and we used the convolution theorem. For given n_0 and ℓ_0 , $P(L_T)$ (and then $P(f_T)$) was uniquely determined from $\tilde{P}(s)$ by numerical inversion [33, 34]. For specific values of (N, L, m) , we fitted the parameters n_0 and ℓ_0 by minimizing the squared error between the simulated distribution and $P(f_T)$ (from Eq. (24)) in a grid search. The results are plotted in Figure 4, with the fitted n_0 and ℓ_0 plotted in Figure S3. It can be seen that Eq. (24) captures quite well the unique features of $P(f_T)$ (except in the tail; see Figure S3).

Inspection of the distributions (Figure 4) for several values of N lead to some interesting observations. For small N (e.g., $N \approx 1000$, and for $m = 1\text{cM}$ and

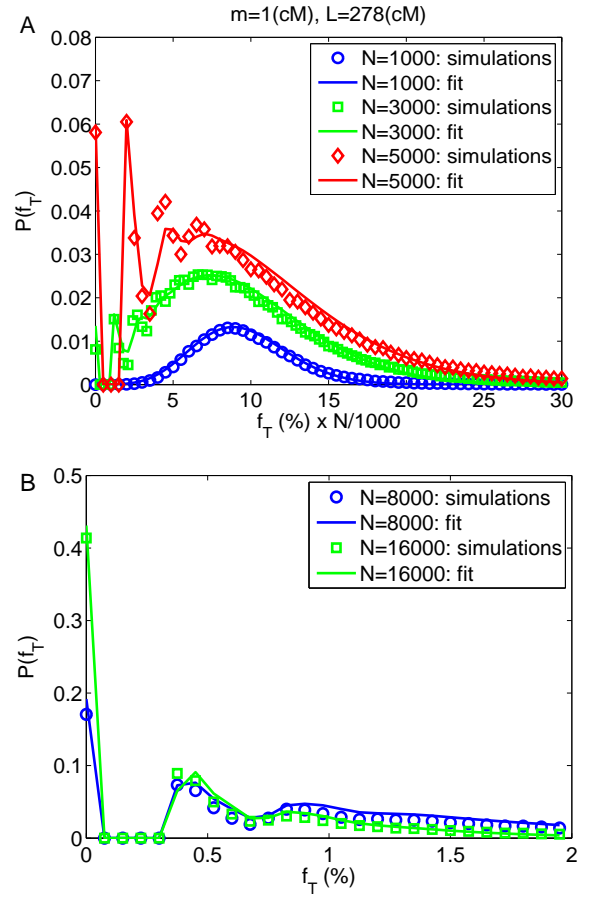


FIG. 4: **The distribution of the total sharing.** Simulation results (symbols) are shown for the distribution of the total sharing between random pairs of individuals in the Wright-Fisher model. Details on the simulation method are as in Figure 2A. **A** The distribution of the total sharing for $N = 1000$, 3000 , and 5000 . For better readability, the x-axis (the total sharing f_T) is given in percentages and scaled by $N/1000$, shifting the distributions for $N = 3000$ and $N = 5000$ to the right. **B** The distribution of the total sharing for $N = 8000$ and 16000 . Here the x-axis is not scaled. In both panels, lines represent the fit to a sum of a Poisson number of shifted exponentials, Eq. (24).

$L = 278\text{cM}$), where the typical amount of sharing is large ($\langle f_T \rangle \approx 5 - 10\%$, $n_0 \approx 10$, $\ell_0 \approx 1\text{cM}$), the distribution is unimodal (but not normal), centered around $\langle f_T \rangle$. As N increases (e.g., $N \approx 3000$), a discontinuous peak appears at $f_T = 0$, with $P(f_T) = 0$ for $0 < f_T < m/L (\approx 0.4\%)$. This is of course due to the restriction on the minimal segment length: a pair of individuals can share either nothing or at least one segment of length m . For $f_T > m/L$ the distribution is continuous, still centered around $\langle f_T \rangle$, but with small, yet notable peaks at $f_T = m/L, 2m/L, 3m/L, \dots$ corresponding to pairs of individuals sharing a small number of minimal length segments. For even larger N (e.g., $N \approx 10000$ and

beyond), $\langle f_T \rangle$ drops below 1%, $n_0 \approx 1$ (ℓ_0 still around 1cM), and the peaks at $f_T = 0$ and $f_T = m/L$ increase such that the distribution decreases almost monotonically beyond m/L . An analytical bound on the fraction of pairs not sharing any segment is given in Supplementary Section S2.3, Eq. S34.

An error model.— To model errors during IBD detection, suppose that we set m large enough as to avoid any false positives (i.e., detected segments that are not truly IBD). We model false negatives as true IBD segments being missed with probability ϵ (independent of the segment length). It is possible to extend the above formulation (Eq. (23)) to the case with errors, as follows. Summing over the true number of segments, n' , the distribution of the number of detected segments, n , is

$$P(n) = \sum_{n'=n}^{\infty} e^{-n_0} \frac{n_0^{n'}}{n!} \binom{n'}{n} (1-\epsilon)^n \epsilon^{n'-n} \\ = e^{-n_0(1-\epsilon)} \frac{[n_0(1-\epsilon)]^n}{n!},$$

that is, a Poisson with parameter $n_0(1-\epsilon)$. Then, as a sum of a random number of independent variables, the mean and variance of L_T are $\langle L_T \rangle = \langle n \rangle \langle \ell \rangle$ and $\text{Var}[L_T] = \langle n \rangle \text{Var}[\ell] + \langle \ell \rangle^2 \text{Var}[n]$, where n is the number of segments and ℓ is the segment length. In our case,

$$\langle L_T \rangle = (1-\epsilon)n_0(\ell_0 + m), \\ \text{Var}[L_T] = (1-\epsilon)n_0[\ell_0^2 + (\ell_0 + m)^2], \quad (25)$$

demonstrating that in the presence of detection errors, both the mean and the variance of the total sharing are $(1-\epsilon)$ times their noise-free values. This is confirmed by simulations in Figure 5.

Other approaches.— We note that a similar approach dates back to R. A. Fisher [35] and others [36–38] in their work on IBD sharing in a model where the population has been recently founded by a number of unrelated individuals. Briefly, those authors too assumed a Poisson number of IBD segments, each of which is exponentially distributed. They then matched the Poisson and exponential parameters to the average IBD sharing and the average number of segments, which they calculated using their population model. Here, we used a different population model (the coalescent; see also Supplementary Section S2.2) and assumed the exponentials have a cutoff at m . In principle, the parameters n_0 and ℓ_0 can also be directly calculated, by matching the mean and variance of the total sharing; see Supplementary Section S2.1. In practice, however, this does not give a good fit. In [10], a similar compound Poisson approach was developed but with a different, coalescent theory-based approximation of the segment length PDF, leading to an improved fit of the remaining parameter n_0 .

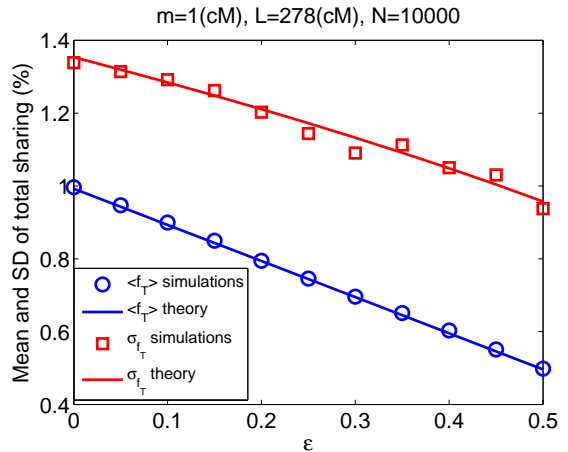


FIG. 5: **The mean and standard deviation (SD) of the total sharing in the presence of detection errors.** Simulation results (symbols) are plotted for mean and SD of the total sharing in the Wright-Fisher model. Simulation details are as in Figure 2, except that each segment was dropped with probability ϵ . Theory is from Eq. (4) for the mean and (12) for the SD, but where the mean is multiplied by $(1-\epsilon)$ and the SD by $\sqrt{1-\epsilon}$, as in Eq. (25).

B. The cohort-averaged sharing

We have so far considered the total sharing between any two random individuals in a population. In practice, we usually collect genetic information on a cohort of n individuals. In this context, we can attribute each individual with the amount of genetic material it shares with the rest of the cohort. Define, for each individual, the *cohort-averaged* sharing \overline{f}_T , as the average total sharing between the given individual and the other $n-1$ individuals in the cohort. Naively, one may anticipate that the width of the distribution of \overline{f}_T will approach zero for large n , because the averaging will tend to eliminate any randomly arising differences between the individuals. We show that in fact, the width of the distribution approaches a non-zero limit. The individuals at the right tail of the cohort-averaged sharing distribution can be seen as “hyper-sharing”, meaning they are, on average, more genetically similar to members of the population than are others. Similarly, individuals at the left tail are “hypo-sharing”. The existence of hyper-sharing individuals is important for prioritizing individuals for sequencing, as we will show in Section IIC.

Define the fraction of the genome shared by individuals i and j as $f_T^{(i,j)}$. The cohort-averaged sharing of i , $\overline{f}_T^{(i)}$, is

$$\overline{f}_T^{(i)} \equiv \frac{1}{n-1} \sum_{j=1, j \neq i}^n f_T^{(i,j)}.$$

The variance of $\overline{f_T^{(i)}}$ is

$$\begin{aligned} \text{Var} \left[\overline{f_T^{(i)}} \right] &= \frac{1}{(n-1)^2} \sum_{j=1, j \neq i}^n \text{Var} \left[f_T^{(i,j)} \right] \\ &+ \frac{1}{(n-1)^2} \sum_{j_1 \neq i} \sum_{j_2 \neq i, j_1} \text{Cov} \left[f_T^{(i,j_1)}, f_T^{(i,j_2)} \right] \\ &= \frac{\sigma_{f_T}^2}{n-1} + \frac{n-2}{n-1} \text{Cov} \left[f_T^{(1,2)}, f_T^{(1,3)} \right] \\ &\approx \frac{\sigma_{f_T}^2}{n} + \text{Cov} \left[f_T^{(1,2)}, f_T^{(1,3)} \right], \end{aligned} \quad (26)$$

where we assumed $n \gg 1$ and we used the fact that the covariance term is identical for all (i, j_1, j_2) combinations and therefore, for simplicity of notation, we set $i = 1$, $j_1 = 2$, and $j_2 = 3$. Recall that $f_T^{(i,j)} = \frac{1}{M} \sum_{s=1}^M I(s)$ (Eq. (3)), where $I(s)$ is the indicator that site s is on a shared segment. Thus, the covariance can be written as

$$\begin{aligned} \text{Cov} \left[f_T^{(1,2)}, f_T^{(1,3)} \right] &= \\ &= \frac{1}{M^2} \sum_{s_1=1}^M \sum_{s_2=1}^M \left[\left\langle I^{(1,2)}(s_1) I^{(1,3)}(s_2) \right\rangle - \pi^2 \right] \\ &\approx \frac{2}{M^2} \sum_{k=1}^M (M-k) \left[\pi_2^{(1,2;1,3)}(k) - \pi^2 \right], \end{aligned}$$

where $I^{(i,j)}(s)$ is the indicator that site s is on a segment shared between individuals i and j , and $\pi_2^{(1,2;1,3)}(k)$ is the probability that a given site is on a segment shared between 1 and 2 and that another site, k markers away from the first, is on a segment shared between 1 and 3. As in Section II A 4 (e.g., Eq. (15)), we will keep only the most dominant term in the sum. Consider the coalescent tree relating the three individuals 1, 2, and 3, and assume that the distance between the sites is $d > m$. If there was no recombination event in the entire tree between the two sites, then immediately $\pi_2^{(1,2;1,3)}(k) = 1$. Otherwise, we assume that each of the two sites belongs to a shared segment (or not) independently of the other, that is, $\pi_2^{(1,2;1,3)}(k) \approx \pi^2$. The probability of no recombination, p_{nr} , depends on T_3 , the total size of the tree of three lineages. Since the PDF of T_3 is $P(T_3) = e^{-T_3/2} - e^{-T_3}$ [24, 39],

$$p_{\text{nr}} = \int_0^\infty P(T_3) e^{-dNT_3/100} dT_3 = \frac{5000}{(50 + dN)(100 + dN)},$$

or, for $dN \gg 100$,

$$p_{\text{nr}} \approx \frac{5000}{(dN)^2}.$$

The covariance becomes

$$\begin{aligned} \text{Cov} \left[f_T^{(1,2)}, f_T^{(1,3)} \right] &\approx \frac{2}{M^2} \sum_{k=m}^M (M-k) \frac{5000}{(k \frac{L}{M} N)^2} \\ &\approx \frac{10000}{N^2 L^2} \int_{m/L}^1 \frac{1-x}{x^2} dk = \frac{10000}{N^2 L^2} \left[\frac{L}{m} - 1 - \ln \left(\frac{L}{m} \right) \right] \\ &\approx \frac{10000}{N^2 m L}. \end{aligned} \quad (27)$$

Substituting Eqs. (15) and (27) in Eq. (26), the standard deviation of the cohort-averaged sharing is

$$\begin{aligned} \sigma_{\overline{f_T}} &\approx \frac{\sigma_{f_T}}{\sqrt{n}} \sqrt{1 + \frac{n}{\sigma_{f_T}^2} \frac{10000}{N^2 m L}} \\ &\approx 10 \sqrt{\frac{\ln \left(\frac{L}{m} \right)}{n N L} \left[1 + \frac{100n}{N m \ln \left(\frac{L}{m} \right)} \right]}. \end{aligned} \quad (28)$$

For $(2 \leq) n \ll Nm \ln \left(\frac{L}{m} \right) / 100$, $\sigma_{\overline{f_T}} \approx \frac{\sigma_{f_T}}{\sqrt{n}}$, while for $n \gg Nm \ln \left(\frac{L}{m} \right) / 100$ (but $< N$, as the size of the cohort cannot exceed the population size), $\sigma_{\overline{f_T}} \approx \frac{100}{N \sqrt{m L}}$, which is independent of n . This implies that even for very large cohorts, the distribution of the cohort-averaged sharing retains a minimal width. Eq. (28) is in good agreement with simulations, as shown in Figure 6A (although some deviations are seen for larger n). We note that the variance was computed for a given individual over all ancestral processes of a cohort of size n . Therefore, the variance within the cohort, for a given ancestral process might actually be smaller. Simulations results (Figure S5), however, show that unless n is very small, Eq. (28) is a good approximation also for the variance within the cohort.

For a genome with c chromosomes,

$$\text{Var} \left[\overline{f_T} \right] = \frac{\sum_{i=1}^c L_i^2 \text{Var} \left[\overline{f_{T,(i)}} \right]}{\left(\sum_{i=1}^c L_i \right)^2},$$

where $\overline{f_{T,(i)}}$ is the cohort-averaged sharing of chromosome i . For the human genome and for small n and $m \approx 1\text{cM}$, Eq. (16) gives

$$\sigma_{\overline{f_T}} \approx \frac{0.382}{\sqrt{nN}}, \quad (29)$$

whereas for large n , Eq. (27) gives

$$\sigma_{\overline{f_T}} \approx \frac{1.68}{N \sqrt{m}}, \quad (30)$$

which is, as explained above, independent of n .

The fact that the width of the cohort-averaged sharing distribution does not approach zero for large n results from the “long-range” correlations between the averaged $(n-1)$ variables, or in other words, the fact that $\text{Cov} \left[f_T^{(i,j_1)}, f_T^{(i,j_2)} \right] > 0$ for all i, j_1, j_2 . In [40], it was

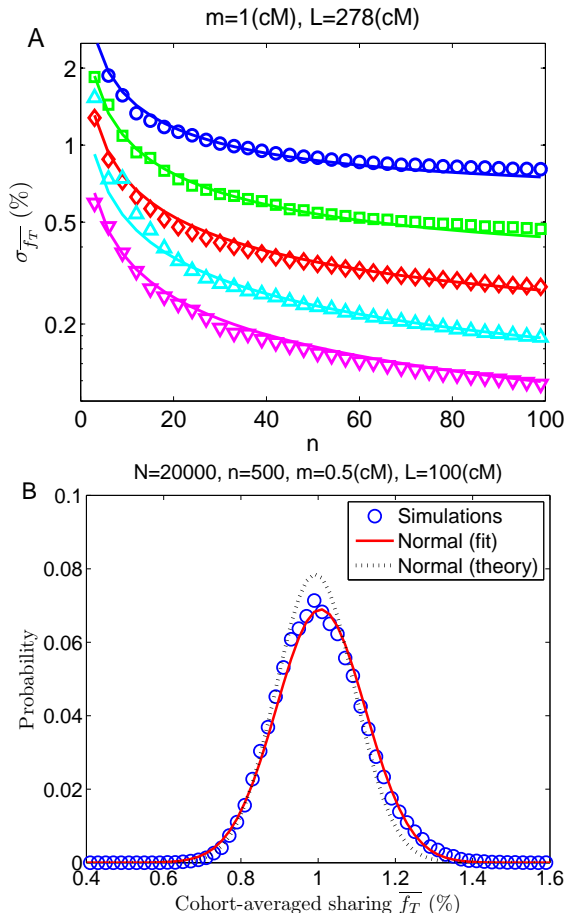


FIG. 6: **The cohort-averaged sharing.** **A** Simulation results (symbols) for σ_{f_T} , that is, the standard deviation (SD) of the cohort-averaged sharing (in percentage of the chromosome) vs. the cohort size n . The different curves correspond to different values of N (top to bottom: $N = 1000, 2000, 4000, 8000, 16000$). The lines correspond to Eq. (28). Details on the simulations are as in Figure 2A. **B** The distribution of the cohort-averaged sharing. The fit is to a normal distribution having the same mean and SD as the real data. Also plotted is a normal distribution with mean given by Eq. (4) and SD given by Eq. (28).

calculated that when all pairs of random variables are weakly correlated, the PDF of their average converges to a normal distribution. In our case, the covariance is $\approx \frac{10000}{N^2 m L}$ (Eq. (27)), much smaller, for typical values of N , L , and m , than $\sigma_{f_T} \approx \frac{100}{NL} \ln\left(\frac{L}{m}\right)$ (Eq. (15)). The variables we average are therefore weakly dependent, as we also observe in simulations (Figure S6). We thus conjectured that the distribution of the cohort-averaged sharing is normal or is close to one. This is confirmed by simulation results, as shown in Figure 6B. We note, however, that a small but systematic deviation from a normal distribution exists in all parameter configurations we tested, in the form of a broader right tail and a narrower left tail than expected (Figure S6). This seems to

be due to the small probability ($\approx 1/N$) of random pairs of individuals to be close relatives.

C. Implications to sequencing study design

Suppose we have sparse genotype information for a large cohort, as well as whole-genome sequences for a subset of it. If the genotype data allow detection of IBD shared segments, then alleles not typed can be directly imputed if they lie on haplotypes shared with sequenced individuals (see, e.g., [22]). In fact, such a strategy is expected to be quite successful; as we mentioned in Section II A 1, only about one recent mutation is expected on each shared segment. Since some individuals share more than others, their sequencing should be prioritized if imputation power is to be maximized. Recently, Gusev et al. [17] developed an algorithm (INFOTIP) for sample selection based on the observed IBD sharing. Here, using our results in Section II B, we calculate the theoretical maximal imputation power.

Assume first that individuals are haploids; the case of diploids is treated later. Assume a cohort of size n , a budget that enables the sequencing of n_s individuals, and two selection strategies: either of random n_s individuals or of the n_s individuals with the largest cohort-averaged sharing. Define an imputation metric, $p_c^{(i)}$, as the average fraction of the genome of i , an individual not sequenced, that is shared IBD with at least one sequenced individual. Let the selected individuals be m_1, m_2, \dots, m_{n_s} , and denote the fraction of the genome that i shares with m_j as $f_T^{(i, m_j)}$. To calculate $p_c^{(i)}$, we assume that for all $j_1, j_2 = 1, \dots, n_s$ ($j_1 \neq j_2$), $f_T^{(i, m_{j_1})}$ is independent of $f_T^{(i, m_{j_2})}$ (which is justified, as we showed in Section II B). We also assume that the locations of the shared segments are independent and uniformly distributed along the genome. Under these assumptions, the probability of a locus to be covered by at least one sequenced individual is

$$p_c^{(i)} = 1 - \prod_{j=1}^{n_s} \left(1 - f_T^{(i, m_j)}\right), \quad (31)$$

and this is also the covered fraction of the genome. We note, however, that assuming that the locations of shared segments are independent and uniformly distributed is mostly for mathematical convenience. Simulation results (Figure S7) show that sharing tends to concentrate at specific loci, implying that Eq. (31) can be thought of as an upper bound (see Figure 7). When $f_T \ll 1$,

$$p_c^{(i)} \approx 1 - \exp \left[- \sum_{j=1}^{n_s} f_T^{(i, m_j)} \right],$$

and for random selection of individuals for sequencing,

$$p_c^{(\text{rand})} \approx 1 - \exp(-n_s \langle f_T \rangle), \quad (32)$$

where $\langle f_T \rangle$ is given by Eq. (4). When selecting the highest sharing individuals, values of $f_T^{(i,m_j)}$ come from the right tail of the cohort-averaged sharing distribution, $P(f_T)$,

$$\sum_{j=1}^{n_s} f_T^{(i,m_j)} \approx n_s \frac{\int_{\bar{f}_c}^{\infty} \bar{f}_T P(\bar{f}_T) d\bar{f}_T}{\int_{\bar{f}_c}^{\infty} P(\bar{f}_T) d\bar{f}_T} \equiv n_s \langle f_T^{(\text{high})} \rangle,$$

where \bar{f}_c and $\langle f_T^{(\text{high})} \rangle$ are the minimum and average, respectively, of the cohort-averaged sharing among the sequenced individuals ($\int_{\bar{f}_c}^{\infty} P(\bar{f}_T) d\bar{f}_T = n_s/n$). Since we argued in Section IIB that $P(\bar{f}_T)$ is approximately normal with parameters $\langle f_T \rangle$ and $\sigma_{\bar{f}_T}$ (Eq. (28)), \bar{f}_c satisfies

$$\text{erfc} \left[\frac{\bar{f}_c - \langle f_T \rangle}{\sqrt{2}\sigma_{\bar{f}_T}} \right] = 2n_s/n. \quad (33)$$

We can thus finally write

$$p_c^{(\text{high})} \approx 1 - \exp \left(-n_s \langle f_T^{(\text{high})} \rangle \right). \quad (34)$$

Before getting to simulations, we notice that in practice, selection of *exactly* those individuals with the largest cohort-averaged sharing will not achieve the imputation power of Eq. (34). This is because the top sharing individuals usually share many segments with each other and thus sequencing of all of them will be redundant (e.g., in the extreme case of siblings, both will appear as top sharing, but sequencing of both will add little power beyond sequencing just one). To avoid such redundancies, we selected the high-sharing (simulated) individuals using INFOSTIP [17], which proceeds in a greedy manner, each time selecting the individual who shares the most with the rest of the cohort in regions that are not yet covered by the already selected individuals. We then compared the imputation power when individuals were selected either randomly or using INFOSTIP. The results, shown in Figure 7, suggest good agreement between the theoretical Eqs. (32) and (34) and the simulations, at least as long as n_s is not large (relative to n). For large n_s , the coverage is lower than predicted, likely due to the non-uniform concentration of the shared segments.

For a cohort of n diploid individuals (assuming phase can be resolved) we redefine the cohort-averaged sharing as

$$\overline{f_{T,\text{dip}}}^{(i)} \equiv \frac{1}{2} \left(\overline{f_T}^{(i,1)} + \overline{f_T}^{(i,2)} \right),$$

(where, e.g., $\overline{f_T}^{(i,1)}$ is the cohort-averaged sharing of the first chromosome of individual i) and assume that the individuals selected for sequencing have the largest diploid cohort-averaged sharing. Since the two terms in $\overline{f_{T,\text{dip}}}^{(i)}$ are weakly dependent,

$$\sigma_{\overline{f_{T,\text{dip}}}}(n) \approx \frac{1}{\sqrt{2}} \sigma_{\bar{f}_T}(2n),$$

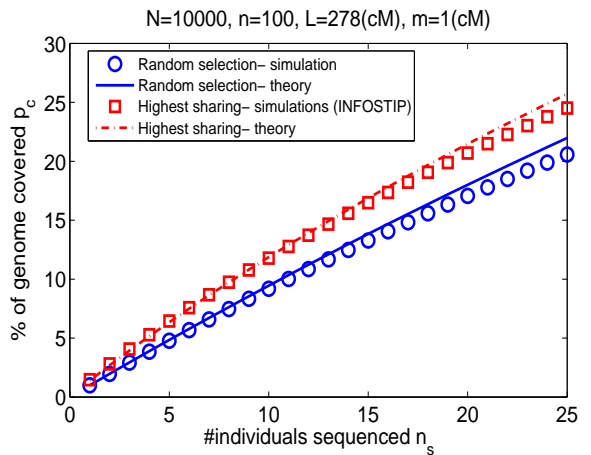


FIG. 7: **Coverage of genomes not selected for sequencing by IBD shared segments.** We simulated 500 Wright-Fisher populations with $N = 10000$, $n = 100$, and $L = 278\text{cM}$, and searched for IBD segments with length $\geq m = 1\text{cM}$. For each plotted data point, we selected n_s individuals either randomly or using INFOSTIP. Then, for each of the $n - n_s$ individuals not selected, we calculated the fraction of their genomes shared with at least one selected individual. We plot (symbols) the average coverage over all individuals in all populations. Lines correspond to theory: Eq. (32) for random selection and Eq. (34) for INFOSTIP selection.

where $\sigma_{\bar{f}_T}$ is given by Eq. (28). The coverage metric p_c is interpreted, as before, as the probability of a locus on a given chromosome to be in a segment shared with at least one sequenced chromosome. The theory developed above is still valid, provided that in Eqs. (32) and (34) n_s is replaced by $2n_s$ and that in Eq. (33) $\sigma_{\bar{f}_T}$ is replaced by $\sigma_{\overline{f_{T,\text{dip}}}}$.

Increase in association power.— Using our results for the power of imputation by IBD, we calculate below the expected subsequent increase in power to detect rare variant association. We use the simple model of [41], in which we consider rare variants that appear in cases but not in any control, and assume that the causal variant is dominant.

Assume that we have genotyped and detected IBD segments in a cohort of n_c (diploid) cases and n_t controls, and that we sequenced a subset of n_s individuals, out of which $n_{c,s}$ are cases and $n_{t,s}$ are controls ($n_s = n_{c,s} + n_{t,s}$). After imputation by IBD, a locus in a (diploid) individual not sequenced has probability p_c^2 to be successfully imputed, where p_c is given by Eq (32) or Eq. (34). For a given locus, we define the *effective* number of cases (controls), as the number of cases (controls) for which genotypes are known either directly from sequencing or from imputation. Since there are $n_c - n_{c,s}$ cases not sequenced and $n_t - n_{t,s}$ controls not sequenced,

$$\begin{aligned} n_c^{(\text{eff})} &\approx n_{c,s} + (n_c - n_{c,s})p_c^2, \\ n_t^{(\text{eff})} &\approx n_{t,s} + (n_t - n_{t,s})p_c^2. \end{aligned} \quad (35)$$

In the last equation we assumed, without loss of generality, that cases can only be imputed using other cases, and vice versa. The probability of a variant to appear in exactly b cases but in no controls, under the null hypothesis that the variant assort independently of the disease, is given by Fisher's exact test,

$$P(\text{cases only}) = \binom{n_c^{(\text{eff})}}{b} / \binom{n_c^{(\text{eff})} + n_t^{(\text{eff})}}{b}.$$

Define Q as the threshold P-value and denote by b^* the smallest integer above which $P(\text{cases only}) < Q$. When the causal variant carrier frequency in cases is β , the probability of the variant to appear in b cases is binomial, and the power is, for a given Q ,

$$\Pi = \sum_{b=b^*}^{n_c^{(\text{eff})}} \binom{n_c^{(\text{eff})}}{b} \beta^b (1-\beta)^{n_c^{(\text{eff})}-b}. \quad (36)$$

In Figure S8, we plot the power vs. $n_{c,s}$, when the sequencing budget $n_s = n_{c,s} + n_{t,s}$ is fixed and for representative parameter values. In Figure 8, we plot the power vs. the carrier frequency for the optimal value of $n_{c,s}$. The figure demonstrates that the power increases by several fold when imputation by IBD is used. This is, however, an expected consequence of increasing the effective sample size, and would likely be achieved with any imputation algorithm (e.g., [42]). The figure also shows an additional, slight increase when the highest sharing individuals are selected for sequencing. Thus, while it should be easy to identify the highest sharing individuals given a genotyped cohort (e.g., using INFOSTIP [17]), and doing so will increase the association power, our results suggest that the gain in power over a random selection will be minor.

D. Other applications of the variance of IBD sharing

1. An estimator of the population size

Assume that we have genotyped or sequenced a diploid chromosome of one individual and calculated f_T , the fraction of the chromosome shared between the individual's paternal and maternal chromosomes. Can we estimate the effective population size?

According to Eq. (4), $\langle f_T \rangle = \frac{100(25+Nm)}{(50+Nm)^2}$. Solving for N gives (see also [10]),

$$N = \frac{50}{m \langle f_T \rangle} \left[(1 - \langle f_T \rangle) + \sqrt{1 - \langle f_T \rangle} \right] \approx \frac{100}{m \langle f_T \rangle} - \frac{75}{m},$$

for $\langle f_T \rangle \ll 1$. This suggests the following estimator,

$$\hat{N} = \frac{100}{m f_T} - \frac{75}{m}. \quad (37)$$

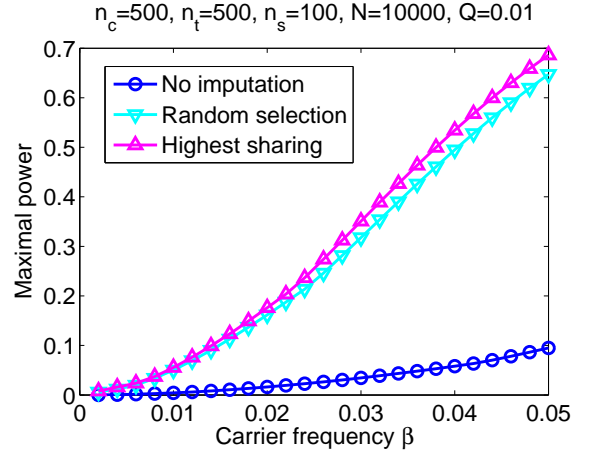


FIG. 8: Power to detect an association after imputation by IBD. The figure shows the maximal power to detect an association, with and without imputation by IBD, and with sequenced individuals selected either randomly or according to their total sharing. The parameters we used were: $N = 10000$, $L = 278\text{cM}$ (one chromosome), $m = 1\text{cM}$, cohort size of 500 cases and 500 controls, a total sequencing budget of $n_s = 100$ individuals, and a threshold P-value of $Q = 0.01$. For each carrier frequency β , we computed the power for each pair of $n_{c,s}$ and $n_{t,s}$ (number of sequenced cases and controls, respectively) such that $n_{c,s} + n_{t,s} = n_s$, and recorded and plotted the maximal power. The power was calculated using Eqs. (35) and (36), where in Eq. (35), p_c was set to zero for the case of no imputation, or calculated using Eqs. (32) and (34) (random selection and selection by total sharing, respectively, and adjusted for diploid individuals). For the studied parameter set, imputation by IBD leads to a major increase in power. Proper selection of individuals for sequencing also contributes to the power but only slightly.

Below, we investigate the properties of the simple estimator of Eq. (37). Using Jensen's inequality, it is easy to see that the estimator is biased,

$$\langle \hat{N} \rangle = \frac{100}{m} \left\langle \frac{1}{f_T} \right\rangle - \frac{75}{m} \geq \frac{100}{m \langle f_T \rangle} - \frac{75}{m} = N.$$

The variance of \hat{N} is proportional to $\text{Var}[1/f_T]$, which we could not calculate, but could approximate as follows. Let us write \hat{N} as

$$\begin{aligned} \hat{N} &= \frac{100}{m[(f_T - \langle f_T \rangle) + \langle f_T \rangle]} - \frac{75}{m} \\ &\approx \frac{100}{m \langle f_T \rangle} \left(1 - \frac{f_T - \langle f_T \rangle}{\langle f_T \rangle} \right) - \frac{75}{m}, \end{aligned}$$

where we applied the Taylor expansion $\frac{1}{1+x} \approx 1 - x$, assuming $|f_T - \langle f_T \rangle| \ll \langle f_T \rangle$ (in which regime clearly $\langle \hat{N} \rangle = N$). Since additive constants do not contribute to the variance, the standard deviation is

$$\sigma_{\hat{N}} \approx \frac{100\sigma_{f_T}}{m \langle f_T \rangle^2} \approx \frac{mN^{3/2}}{10} \sqrt{\frac{\ln(L/m)}{L}},$$

where we used $\langle f_T \rangle \approx 100/(mN)$ (Eq. (4)), and Eq. (15)) for σ_{f_T} . The effective population size can also be inferred using Watterson's estimator, which is $\hat{N}_W = S_2/(2\mu)$, where S_2 is the number of heterozygous sites and μ is the mutation rate (per chromosome per generation). Watterson's estimator is unbiased, $\langle \hat{N}_W \rangle = N$, and has variance $\text{Var}[\hat{N}_W] = [2\mu N + (2\mu N)^2]/4\mu^2 \approx N^2$. Therefore, $\sigma_{\hat{N}_W}/N \approx 1$, compared to $\sigma_{\hat{N}}/N \approx N^{1/2}$ for the IBD estimator.

Note that in practice, the proposed estimator is not very useful, as it diverges whenever $f_T = 0$ (which is common for large N). Suppose, however, that we have sequences for n (haploid) chromosomes, and that we have computed the total sharing between all pairs. Define $\overline{f_T} = \sum_i \sum_{j>i} f_T^{(i,j)}/\binom{n}{2}$. The estimator now takes the form

$$\hat{N} = \frac{100}{m\overline{f_T}} - \frac{75}{m}. \quad (38)$$

This is again an overestimate, $\langle \hat{N} \rangle \geq N$. In Supplementary Section S3, we show that $\sigma_{\hat{N}}$ is approximately

$$\sigma_{\hat{N}} \approx \frac{mN^{3/2}}{5\sqrt{nL}} \sqrt{\frac{\ln(\frac{L}{m})}{2n} + \frac{100}{Nm}}, \quad (39)$$

For comparison, in Watterson's estimator for n (haploid) chromosomes, $\sigma_{\hat{N}_W}/N \approx 1/\ln n$ (for large N and n), which decays to zero with increasing n slower than the IBD estimator. Simulation results, shown in Figures S9 and S10, confirm the accuracy of Eq. (39) and show that the bias is limited to very small values of n .

In the context of the error model of Section II A 5, introducing a probability ϵ to miss a true IBD segment will decrease the average total sharing by $(1 - \epsilon)$ (Eq. (25)). Consequently, Eq. (38) will estimate a population size approximately $1/(1 - \epsilon)$ ($\approx (1 + \epsilon)$ for small ϵ) larger than the true one.

2. IBD sharing between siblings

The total IBD sharing between relatives can usually be decomposed into sharing due to the recent co-ancestry and “background” sharing due to population inbreeding [13, 14]. While much is known about the distribution of sharing in pedigrees (e.g., [43]), less is known about the population level sharing, and relatedness detection algorithms (e.g., [13, 14]) estimate it empirically. In a different domain, the variance in sharing between relatives appears in theoretical calculations of the variance of heritability estimators [44]. Our results for the variance of the total sharing in the Wright-Fisher model (Section II A) can thus have practical applications if modified to account for recent co-ancestry.

Here, we calculate the variance of the sharing between siblings by combining the approach of [44] with that of

our Section II A 4. Assume that two individuals are siblings, either half or full—we will calculate, without loss of generality, only the sharing between the two chromosomes that descended from the same parent—and denote the fraction of sharing as f_S . Assume as before a population of size N and one chromosome of length L . For a given marker to be on a shared segment, it can either be on a segment directly co-inherited from the same grandparent (probability $1/2$), or otherwise on a segment shared between the grandparents (probability $\pi/2$, Eq. (2)). We ignore boundary effects near the sites of recombination at the parent. The mean fraction of the genome shared is therefore just $\langle f_S \rangle = (1 + \pi)/2$. The variance can be written as in Section II A 4,

$$\text{Var}[f_S] \approx \frac{2}{M^2} \sum_{k=1}^M (M - k) \left[\pi_{2,S}(k) - \frac{1}{4}(1 + \pi)^2 \right],$$

where $\pi_{2,S}(k)$ is the probability of two sites separated by k markers (or genetic distance $d = k\frac{L}{M}$) to be on segments shared between the siblings. The probability that the two sites are both co-inherited from the same grandparent is

$$p_{\text{same}} = \frac{1}{2} [(1 - r)^2 + r^2] = \frac{1}{4} (1 + e^{-d/25}),$$

where r is the recombination fraction and we used Haldane's map function [44]. Also with probability p_{same} , the sites are both inherited from different grandparents, and we use the expressions developed in Section II A 4 for the probability of the sites to be in shared segments: $\pi_{2,S}(k) = \pi^2 + \Theta(d - m)p_{\text{nr}}$ (where $p_{\text{nr}} \approx 50/(Nd)$ and $\Theta(x) = 1$ for $x > 0$ and is zero otherwise). With probability $(1 - 2p_{\text{same}})$, one site is co-inherited and the other is not; in that case $\pi_{2,S}(k) = \pi$. Approximating the sum as an integral and simplifying, we finally have

$$\text{Var}[f_S] \approx 2 \int_0^1 dx (1 - x) \left\{ \frac{\pi (1 - e^{-xL/25})}{2} + \frac{1 + e^{-xL/25}}{4} \left[1 + \pi^2 + \Theta\left(x - \frac{m}{L}\right) \frac{50}{NxL} \right] - \frac{(1 + \pi)^2}{4} \right\}. \quad (40)$$

We solved Eq. (40) using MATHEMATICA and summed over all chromosomes as in Eq. (5). The results for the mean and standard deviation (SD) of the total sharing between siblings are plotted in Figure 9 and compared to an outbred population where the grandparents are unrelated. The SD in the outbred population overestimates the Wright-Fisher SD, in up to $\approx 18\%$ for N as small as 500.

3. IBD sharing after an admixture pulse

In this final subsection, we study the IBD sharing in a simple admixture model. In our model, a single population A of constant size N has received gene flow from

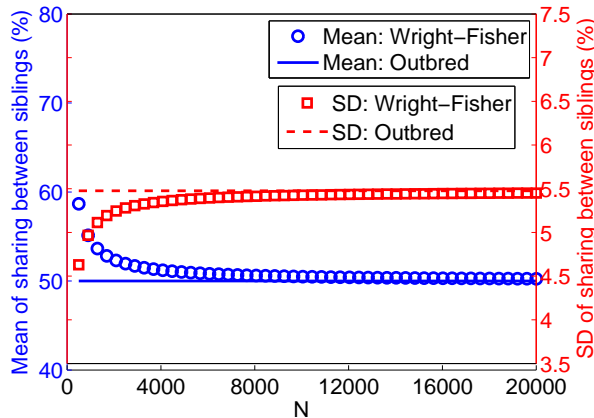


FIG. 9: **IBD sharing between siblings in the Wright-Fisher model.** We plot the theoretical mean and standard deviation (SD) of the IBD sharing between the (maternal only or paternal only haploid) genomes of siblings. Lines correspond to an outbred population (unrelated grandparents): the mean sharing is 50% and the SD is taken from [44]. Symbols correspond to the theory for Wright-Fisher model: the mean sharing is $(1 + \pi)/2$ (where π is given by Eq. (2)), and the SD is given by Eq. (40). We used $m = 1\text{cM}$ and the chromosome lengths of the autosomal human genome. Note that the y-axis is on the left side for the mean and on the right side for the SD.

population B , G_a generations ago. We assume that gene flow took place for one generation only (hence, an admixture pulse), and further, that population B is sufficiently large that the chromosomes it donated to A share no detectable IBD segments. Denote the fraction of the lineages coming from population A at the admixture event as α (fraction $1 - \alpha$ coming from B), and let $T_a = G_a/N$ be the scaled admixture time. We are interested in IBD sharing between extant chromosomes in population A .

To approximate the mean IBD sharing in the sample, note that if admixture was very recent, then two chromosomes will be potentially shared only if both descend from population A , which occurs with probability α^2 . Therefore, the mean sharing is α^2 times its value without admixture. While this is a good approximation (Figure S11), it does not account for two chromosomes, one or two of which are from the external population B , having their common ancestor more recently than the admixture event. We therefore calculate the mean IBD sharing using Eq. (17), using the following (non-normalized) PDF for the coalescence times:

$$\Phi(t) = \begin{cases} e^{-t} & t < T_a, \\ \alpha^2 e^{-t} & t > T_a, \end{cases} \quad (41)$$

which gives

$$\begin{aligned} \langle f_T \rangle &= \int_0^\infty \Phi(t) \left(1 + \frac{mNt}{50} \right) e^{-\frac{mNt}{50}} dt \\ &= \alpha^2 \frac{100(25 + mN)}{(50 + mN)^2} + T_a(1 - \alpha^2) + \mathcal{O}(T_a^2). \end{aligned} \quad (42)$$

Note that this is just $\langle f_T \rangle_{\text{admixture}} \approx \alpha^2 \langle f_T \rangle_{\text{no admixture}} + (1 - \alpha^2)T_a$. The first term corresponds to lineages descending from population A ; the second term corresponds to at least one of the lineages descending from population B but where the lineages have coalesced already in the hybrid population. The variance can be similarly calculated, by substituting Eq. (41) into Eq. (19),

$$\begin{aligned} \text{Var}[f_T] &\approx 2 \int_{m/L}^1 (1-x) \left[\int_0^{T_a} e^{-t-txNL/50} dt \right] dx \\ &+ 2\alpha^2 \int_{m/L}^1 (1-x) \left[\int_{T_a}^\infty e^{-t-txNL/50} dt \right] dx \\ &\approx \frac{100}{NL} \left\{ \ln\left(\frac{L}{m}\right) - 1 + (1 - \alpha^2) \left[\gamma - \left| \ln\left(\frac{mNT_a}{50}\right) \right| \right] \right\}, \end{aligned} \quad (43)$$

where γ is the Euler-Mascheroni constant, and we solved the integrals in MATHEMATICA and later simplified under specific assumptions (see Supplementary Section S4). Eq. (43) usually predicts a variance slightly smaller than the case of no admixture. Simulation results are shown in Figure S11 for the mean and variance. While agreement is not perfect (as Eq. (19) is itself approximate), Eqs. (42) and (43) capture the main effects of changing α and T_a . Note that the result of Eq. (42) implies that, for small T_a and large N , the observed mean IBD sharing is as if the population is of size $\approx N/\alpha^2$.

A test for admixture.— For recent admixture (small T_a), the fractions of ancestry vary among individuals [45, 46]. In our model, since a pair of segments is shared mostly when both descend from population A , some individuals will share more than others merely due to having a larger fraction of A ancestry. In turn, this will increase the variance of the cohort-averaged sharing. This observation suggests the following test for a recent gene flow into a population. (i) Extract IBD segments and calculate the mean fraction of total sharing over all pairs, $\overline{f_T}$, as well as the SD of the cohort-averaged sharing, $\sigma_{\overline{f_T}}$. (ii) Use Eq. (38) to infer the population size: $\hat{N} = 100/(m\overline{f_T}) - 75/m$. (iii) Simulate N_{pop} populations of size \hat{N} ; extract IBD sharing and calculate the SD of the cohort-averaged sharing in each population. (iv) The P-value for rejecting the null hypothesis of no admixture is the fraction of the N_{pop} populations where the SD of the cohort-averaged sharing was larger than the observed one. Note that the identity of the external population need not be known, nor are the admixture fraction and time; the test relies on admixture creating a gradient of ancestry fractions and hence an increased

variability in the similarity between individuals. Simulation results are plotted in Figure S11, showing that for a P-value of 0.05 and $G_a = 5$, gene flow with $\alpha \approx 0.9$ or lower can be detected ($\alpha \approx 0.8$ or lower for $G_a = 10$). We stress that a broader than expected distribution of cohort-averaged sharing does not *necessarily* indicate admixture, and there might be other factors responsible for the effect (see also the Discussion). We validated, however, that IBD detection errors alone (as in the model of Section II A 5) as well as variable population size (in a simple two-size model) do not lead to significant P-values in the admixture test (Figure S12).

IBD sharing and admixture in the Ashkenazi Jewish population.— As our final result, we apply the admixture test to the real population of Ashkenazi Jews (AJ). Historical records, and recently also genetic studies, suggest that AJ form a genetically distinct group of likely Middle-Eastern origin. However, the AJ population was also shown to receive a significant amount of gene flow from neighboring European populations [47–51]. We analyzed a dataset of ≈ 2600 AJ, details on which have been published elsewhere [10, 51] and are summarized in the Methods section. To detect IBD shared segments in the AJ population, we used GERMLINE [2]. For 500 individuals on chromosome 1, and with $m = 1\text{cM}$, the average fraction of sharing over all pairs is $\approx 4.4\%$, leading to an estimated population size of $\hat{N} \approx 2200$. The SD of the cohort-averaged sharing is 0.52%, higher than the SD in all 500 populations we simulated with a constant size \hat{N} (typically 0.34%, maximum 0.41%). The recent history of Ashkenazi Jews, however, has likely involved bottlenecks and expansions, different from the constant size assumption. In [10], a population model was inferred based on the fraction of the genome shared at different segment lengths. The model’s best estimate of AJ history is a slow expansion until about 35 generations ago, and then a severe bottleneck (effective population size of just 270) followed a by rapid expansion to a current size of a few millions. As can be seen in Figure 10A and B, the model agrees well with the distribution of the fraction of total sharing over all pairs, but predicts a much narrower distribution of cohort-averaged sharing than the true one. Here too, in none of 100 simulated populations with the inferred demography was the SD of the cohort-averaged sharing as large as in the real data. These results, therefore, suggest (based on the AJ population alone) that the AJ population was the target of a recent gene flow. To confirm that the increase in the variance of the cohort-averaged sharing is due (at least partly) to admixture, we ran an admixture analysis (ADMIXTURE [52]) comparing AJ to HapMap’s CEU [31]. As can be seen in Figure 10C, the fraction of “AJ ancestry” is indeed highly correlated with the cohort-averaged sharing (Pearson’s $r = 0.59$).

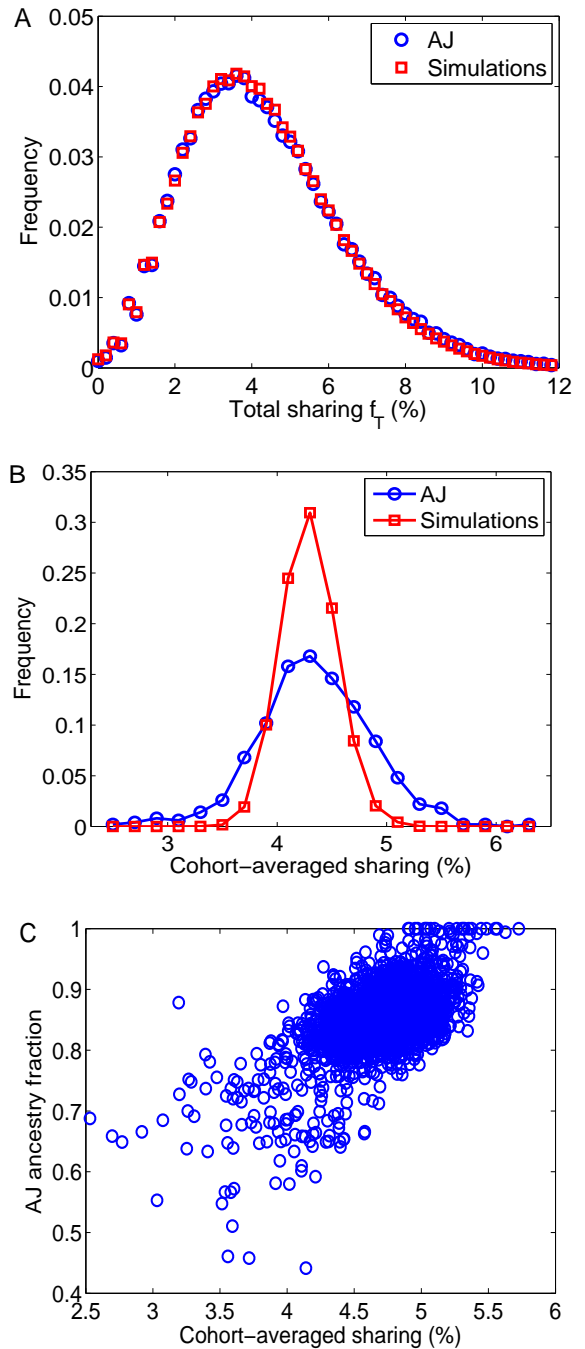


FIG. 10: **IBD sharing and admixture in the Ashkenazi Jewish (AJ) population.** We detected IBD shared segments using GERMLINE in chromosome 1 of $n = 500$ AJ individuals and compared to simulations of the demographic history inferred in [10]. **A** The distribution of the total sharing over all pairs. **B** The distribution of the cohort-averaged sharing. While the demographic model fits well the sharing distribution over all pairs, the distribution of the real cohort-averaged sharing is broader than in the model. **C** We used ADMIXTURE to calculate the admixture fraction of AJ individuals compared to the CEU population. The “AJ ancestry fraction” of each individual is plotted against its cohort-averaged sharing. This panel shows results for the full dataset (≈ 2600 individuals).

III. DISCUSSION

The recent availability of dense genotypes, together with sophisticated detection tools, have transformed IBD sharing into an increasingly important tool in population genetics. Here, we used coalescent theory to compute the variance and other properties of the total sharing in the Wright-Fisher model. For the variance, we suggested three derivations, one of which was more coarse but had a simple closed form that was later extended to populations of variable size. Investigating the cohort-averaged sharing, we discovered the curious phenomenon of ‘hyper-sharing’. We showed how this can be exploited to improve power in imputation and association studies. We also calculated the variance of the total sharing between siblings, and briefly considered some implications to the accuracy of demographic inference. We finally investigated IBD sharing in a hybrid population and suggested a test for admixture based on the cohort-averaged sharing, which we then applied to the Ashkenazi Jewish population. We provide MATLAB routines for the main results.

Most of our analytical results depend on certain assumptions and simplifications, as specified in the individual sections and in Supplementary Section S1.2. Additionally, in reality, the Wright-Fisher model and the coalescent are only approximations of the true ancestral process, and procedures such as phasing, IBD inference, and imputation are also prone to error. IBD detection errors will particularly affect our results for imputation and association studies (Section II C), and these results should therefore be considered as idealized upper bounds. The error model we introduced, where each IBD segment is missed with a certain probability, gives a sense of the effect of errors. Investigation of more detailed models, e.g., length dependent error rate for segment misdetection or more realistic models for imputation and association studies, is challenging and left for future work.

Prospects of our work are in a few fields. First, as shown in [10], theoretical characterization of IBD sharing can lead to new methods for demographic inference, which are expected to perform particularly well when investigating the recent history of genetic isolates. Here, we expanded the theory of IBD sharing to compute the variance of the total sharing and the cohort-average sharing. This turned useful, for example, when we provided in Section II D 1 expressions for the variance of an estimator of the population size based on the average sharing over all pairs of chromosomes and in Section II D 3, where we described a test for recent admixture. In another domain, understanding the distribution of sharing between relatives can improve the accuracy of relatedness detection (Section II D 2). Other potential applications are in the detection of regions either positively selected or associated with a disease based on excess sharing, although more work is needed for these. Finally, our results provide the first estimate for the potential success of imputation by IBD strategies (Section II C). We note that of

course, once a given cohort has been genotyped, IBD can be calculated directly to estimate the expected success of imputation. However, in many cases, study design takes place before the actual recruiting and genotyping, and then, if a rough estimate of the population size is available, our results can be invoked to estimate the amount of resources needed.

One of our interesting findings was the presence of hyper-sharing individuals. While we did not define the term precisely, we referred to the fact that even for large cohorts, the variance of the cohort-averaged sharing does not decrease below a certain value. This result, while somewhat counterintuitive, follows naturally from the population model. In the real population of Ashkenazi Jews (AJ), we showed that the distribution of the cohort-averaged sharing is even broader, indicating possible admixture, and indeed, we found that the cohort-averaged sharing is highly correlated with the Ashkenazi ancestry fraction. This is not to say that admixture was the only factor shaping the distribution of IBD sharing; other factors such as selection or population substructure could have been playing a role as well. Our results, however, emphasize the importance of reconstructing the AJ demography simultaneously with that of their neighboring populations.

IV. METHODS

Coalescent simulations.— To simulate IBD sharing in the Wright-Fisher model, we used the GENOME haploid coalescent simulator [30]. Recombination in GENOME is discretized to short blocks and mutations (which we ignore in this study) are placed on the simulated branches. In all simulations, we generated one chromosome with recombination rate of 10^{-8} per generation per base-pair and block lengths of 10^4 base-pairs (corresponding to resolution of 0.01cM in the lengths of the shared segments).

IBD sharing in simulations.— We used an add-on to GENOME that returns, for each pair of chromosomes, the locations of all shared segments [10]. In that add-on, a segment is shared as long as the two chromosomes share the same ancestor, even if there was a recombination event within the segment. We calculated, for each pair, the total length of shared segments longer than m , and divided by the chromosome size. For Figures 2-6, we simulated $N_{\text{pop}} \geq 100$ populations and $n = 100$ haploid sequences in each population, and calculated all properties of the total sharing among all $N_{\text{pop}} \binom{n}{2}$ available pairs. For the cohort-averaged sharing, we averaged, for each of the n chromosomes, their sharing to each of the other $n - 1$ chromosomes in the cohort, and then used the $N_{\text{pop}} n$ calculated values to obtain the variance and the distribution. Details on the simulation of an admixture pulse can be found in Supplementary Section S4.

The Ashkenazi Jewish (AJ) cohort.— The cohort we analyzed was previously described in [10, 51]. Briefly, DNA samples from ≈ 2600 AJ were genotyped on

Illumina-1M SNP array. Genotypes (autosomal only) were subjected to quality control, including removal of close relatives, and phasing (BEAGLE [53]), leaving finally $\approx 741,000$ SNPs for downstream analysis. IBD sharing was calculated using GERMLINE [2] with the following parameters: `bits: 25, err_hom: 0, err_het: 2, min_m: 1, h_extend: 1`. The results presented in Section IID3 remained qualitatively the same even when we used a longer length cutoff of $m = 5\text{cM}$.

Admixture analysis.— For the admixture analysis, we merged the HapMap3 CEU population [31] (release 2) with the AJ data, removed all SNPs with potential strand inconsistency, and pruned SNPs that were in linkage disequilibrium [5]. We then ran ADMIXTURE [52] with default parameters and $K = 2$. ADMIXTURE consistently classified all individuals according to their population (CEU/AJ). Genome-wide, the AJ ancestry fraction was $\approx 85\%$, compared to $\approx 3\%$ for the CEU population. Principal components analysis (SMARTPCA [54]) gave qualitatively similar results.

Simulations of AJ demography.— Demographic recon-

struction of the AJ population was performed in [10] using chromosome 1 of 500 randomly selected individuals and using a novel IBD-based method described therein. Simulations presented here were performed using the final set of inferred demographic parameters: ancestral (diploid) population effective size of ≈ 2300 individuals, expansion starting 200 generations ago reaching ≈ 45000 individuals 33 generations ago, a severe bottleneck of ≈ 270 individuals, and an expansion to the current size of ≈ 4.3 million individuals. Simulation of one hundred populations was carried out using GENOME [30].

V. ACKNOWLEDGEMENT

We thank the reviewers for insightful comments and Omer Bobrowski for discussions. S. C. thanks the Human Frontier Science Program for financial support. I. P. acknowledges support from NSF grant CCF 0845677 and NIH grant U54 CA121852.

-
- [1] D. L. Hartl and A. G. Clark. *Principles of population genetics*. Sinauer Associates, 4th edition, 2006.
 - [2] A. Gusev, J. K. Lowe, M. Stoffel, M. J. Daly, D. Altshuler, J. L. Breslow, J. M. Friedman, and I. Pe'er. Whole population, genome-wide mapping of hidden relatedness. *Genome Res.*, 19:318–326, 2009.
 - [3] B. L. Browning and S. R. Browning. A fast, powerful method for detecting Identity by Descent. *Am. J. Hum. Genet.*, 88:173–182, 2011.
 - [4] A. Albrechtsen, T. Sand Korneliussen, I. Moltke, T. van Overseem Hansen, F. Cilius Nielsen, and R. Nielsen. Relatedness mapping and tracts of relatedness for genome-wide data in the presence of linkage disequilibrium. *Genet. Epidemiol.*, 33:266–274, 2009.
 - [5] S. Purcell, N. Neale, K. Todd-Brown, L. Thomas, M. A. R. Ferreira, D. Bender, J. Maller, P. Sklar, P. I. W. de Bakker, M. J. Daly, and P. C. Sham. PLINK: A tool set for whole-genome association and population-based linkage analyses. *Am. J. Hum. Genet.*, 81:559–575, 2007.
 - [6] I. M. Carr, A. F. Markham, and S. D. J. Pena. Estimating the degree of Identity by Descent in consanguineous couples. *Hum. Mutat.*, 32:1350–1358, 2011.
 - [7] M. D. Brown, C. G. Glazner, C. Zheng, and E. A. Thompson. Inferring coancestry in population samples in the presence of linkage disequilibrium. *Genetics*, 190:1447–1460, 2012.
 - [8] A. Kong, G. Masson, M. L. Frigge, A. Gylfason, P. Zemanovich, G. Thorleifsson, P. I. Olason, A. Ingason, S. Steinberg, T. Rafnar, P. Sulem, M. Mouy, F. Jonsson, U. Thorsteinsdottir, D. F. Gudbjartsson, H. Stefansson, and K. Stefansson. Detection of sharing by descent, long-range phasing and haplotype imputation. *Nat. Genet.*, 9:1068–1075, 2008.
 - [9] D. Davison, J.K. Pritchard, and G. Coop. An approximate likelihood for genetic data under a model with recombination and population splitting. *Theor. Popul. Biol.*, 75:331–345, 2009.
 - [10] P. F. Palamara, T. Lencz, A. Darvasi, and I. Pe'er. Length distributions of identity by descent reveal fine-scale demographic history. *Am. J. Hum. Genet.*, 91:809–822, 2012.
 - [11] A. Gusev, P. F. Palamara, G. Aponte, Z. Zhuang, A. Darvasi, P. Gregersen, and I. Pe'er. The architecture of long-range haplotypes shared within and across populations. *Mol. Biol. Evol.*, 29:473–486, 2012.
 - [12] A. Albrechtsen, I. Moltke, and R. Nielsen. Natural selection and the distribution of Identity-by-Descent in the human genome. *Genetics*, 186:295–308, 2010.
 - [13] C. D. Huff, D. J. Witherspoon, T. S. Simonson, J. Xing, W. S. Watkins, Y. Zhang, T. M. Tuohy, D. W. Neklason, R. W. Burt, S. L. Guthery, S. R. Woodward, and L. B. Jorde. Maximum-likelihood estimation of recent shared ancestry (ERSA). *Genome Res.*, 21:768–774, 2011.
 - [14] B. M. Henn, L. Hon, J. M. Macpherson, N. Eriksson, S. Saxonov, I. Pe'er, and J. L. Mountain. Cryptic distant relatives are common in both isolated and cosmopolitan genetic samples. *PLoS One*, 7:e34267, 2012.
 - [15] B. Kirkpatrick, S. Cheng Li, R. M. Karp, and E. Halperin. Pedigree reconstruction using Identity by Descent. *J. Comput. Biol.*, 18:1481–1493, 2011.
 - [16] E. L. Stevens, G. Heckenberg, E. D. O. Roberson, J. D. Baugher, T. J. Downey, and J. Pevsner. Inference of relationships in population data using Identity-by-Descent and Identity-by-State. *PLoS Genet.*, 7:e1002287, 2011.
 - [17] A. Gusev, M. J. Shah, E. E. Kenny, A. Ramachandran, J. K. Lowe, J. Salit, C. C. Lee, E. C. Levandowsky, T. N. Weaver, Q. C. Doan, H. E. Peckham, S. F. McLaughlin, M. R. Lyons, V. N. Sheth, M. Stoffel, F. M. De La Vega, J. M. Friedman, J. L. Breslow, and I. Pe'er. Low-pass genome-wide sequencing and variant inference using Identity-by-Descent in an isolated human population. *Genetics*, 190:679–689, 2012.
 - [18] M. N. Setty, A. Gusev, and I. Pe'er. HLA type inference via haplotypes Identical by Descent. *J. Comput. Biol.*,

- 18:483–493, 2011.
- [19] A. Gusev, E. E. Kenny, J. K. Lowe, J. Salit, R. Saxena, S. Kathiresan, D. M. Altshuler, J. M. Friedman, J. L. Breslow, and I. Pe’er. DASH: A method for Identity-by-Descent haplotype mapping uncovers association with recent variation. *Am. J. Hum. Genet.*, 88:706–717, 2011.
 - [20] N. Akula, S. Detera-Wadleigh, Y. Yao Shugart, M. Nalls, J. Steele, and F. J. McMahon. Identity-by-descent filtering as a tool for the identification of disease alleles in exome sequence data from distant relatives. *BMC Proceedings*, 5:S76, 2011.
 - [21] S. R. Browning and E. A. Thompson. Detecting rare variant associations by Identity-by-Descent mapping in case-control studies. *Genetics*, 190:1521–1531, 2012.
 - [22] L. H. Uricchio, J. X. Chong, K. D. Ross, C. Ober, and D. L. Nicolae. Accurate imputation of rare and common variants in a founder population from a small number of sequenced individuals. *Genet. Epidemiol.*, 36:312–319, 2012.
 - [23] K. Palin, H. Campbell, A. F. Wright, J. F. Wilson, and R. Durbin. Identity-by-Descent-based phasing and imputation in founder populations using graphical models. *Genet. Epidemiol.*, 35:853–860, 2011.
 - [24] J. Wakeley. *Coalescent Theory: An Introduction*. Roberts & Company Publishers, 2009.
 - [25] G. A. T. McVean and N. J. Cardin. Approximating the coalescent with recombination. *Phil. Trans. R. Soc. B*, 360:1387–1393, 2005.
 - [26] R. R. Hudson. Properties of a neutral allele model with intragenic recombination. *Theor. Popul. Biol.*, 23:183–201, 1983.
 - [27] K. T. Simonsen and G. A. Churchill. A Markov chain model of coalescence with recombination. *Theor. Popul. Biol.*, 52:43–59, 1997.
 - [28] Peter Mörters. Lecture notes: Continuous time markov chains.
 - [29] R. C. Griffiths. *The two-locus ancestral graph*, volume 18 of *Selected Proceedings of the Symposium on Applied Probability, Sheffield, 1989. IMS Lecture Notes - Monograph Series*, pages 100–117. Institute of Mathematical Statistics, Hayward, California, 1991.
 - [30] L. Liang, S. Zöllner, and G. R. Abecasis. GENOME: a rapid coalescent-based whole genome simulator. *Bioinformatics*, 23:1565–1567, 2007.
 - [31] The International HapMap Consortium. A second generation human haplotype map of over 3.1 million SNPs. *Nature*, 449:851–861, 2007.
 - [32] H. Li and R. Durbin. Inference of human population history from individual whole-genome sequences. *Nature*, 475:493–496, 2011.
 - [33] K. J. Hollenbeck. INVLAP.M: A matlab function for numerical inversion of Laplace transforms by the de Hoog algorithm. 1998.
 - [34] F. R. de Hoog, J. H. Knight, and A. N. Stokes. An improved method for numerical inversion of Laplace transforms. *SIAM. J. Sci. and Stat. Comput.*, 3:357–366, 1982.
 - [35] R. A. Fisher. A fuller theory of “junctions” in inbreeding. *Heredity*, 8:187–197, 1954.
 - [36] J. H. Bennet. The distribution of heterogeneity upon inbreeding. *J. Roy. Stat. Soc. B Met.*, 16:88–99, 1954.
 - [37] P. Stam. The distribution of the fraction of the genome identical by descent in finite random mating populations. *Genet. Res.*, 35:131–155, 1980.
 - [38] N. H. Chapman and E. A. Thompson. A model for the length of tracts of identity by descent in finite random mating populations. *Theor. Pop. Biol.*, 64:141–150, 2003.
 - [39] C. Wiuf and J. Hein. Recombination as a point process along sequences. *Theor. Popul. Biol.*, 55:248–259, 1999.
 - [40] H. J. Hilhorst and G. Schehr. A note on q -Gaussians and non-Gaussians in statistical mechanics. *J. Stat. Mech.*, page P06003, 2007.
 - [41] Y. Shen, R. Song, and I. Pe’er. Coverage tradeoffs and power estimation in the design of whole-genome sequencing experiments for detecting association. *Bioinformatics*, 27:1995–1997, 2011.
 - [42] B. Howie, C. Fuchsberger, M. Stephens, J. Marchini, and G. R. Abecasis. Fast and accurate genotype imputation in genome-wide association studies through pre-phasing. *Nat. Genet.*, 44:955–959, 2012.
 - [43] W. G. Hill and B. S. Weir. Variation in actual relationship as a consequence of Mendelian sampling and linkage. *Genet. Res.*, 93:47–64, 2011.
 - [44] P. M. Visscher, S. E. Medland, M. A. R. Ferreira, K. I. Morley, G. Zhu, B. K. Cornes, G. W. Montgomery, and N. G. Martin. Assumption-free estimation of heritability from genome-wide identity-by-descent sharing between full siblings. *PLoS Genet.*, 2:e41, 2006.
 - [45] S. Gravel. Population genetics models of local ancestry. *Genetics*, 191:607–619, 2012.
 - [46] P. Verdu and N. A. Rosenberg. A general mechanistic model for admixture histories of hybrid populations. *Genetics*, 189:1413–1426, 2011.
 - [47] H. Ostrer. A genetic profile of contemporary Jewish populations. *Nat. Rev. Genet.*, 2:891–898, 2001.
 - [48] G. Atzmon, L. Hao, I. Pe’er, C. Velez, A. Pearlman, P. F. Palamara, B. Morrow, E. Friedman, C. Oddoux, E. Burns, and H. Ostrer. Abraham’s children in the genome era: Major Jewish diaspora populations comprise distinct genetic clusters with shared middle eastern ancestry. *Am. J. Hum. Genet.*, 86:850–859, 2010.
 - [49] D. M. Behar, B. Yunusbayev, M. Metspalu, E. Metspalu, Saharon Rosset, J. Parik, S. Rootsi, G. Chaubey, I. Kutuev, G. Yudkovsky, E. K. Khusnutdinova, O. Balanovsky, O. Semino, L. Pereira, D. Comas, D. Gurwitz, B. Bonne-Tamir, T. Parfitt, M. F. Hammer, K. Skorecki, and R. Villems. The genome-wide structure of the Jewish people. *Nature*, 466:238–242, 2010.
 - [50] S. M. Bray, J. G. Mulle, A. F. Dodd, A. E. Pulver, S. Wooding, and S. T. Warren. Signatures of founder effects, admixture, and selection in the Ashkenazi Jewish population. *P. Natl. Acad. Sci. USA*, 107:16222–16227, 2010.
 - [51] S. Guha, J. A. Rosenfeld, A. K. Malhotra, A. T. Lee, P. K. Gregersen, J. M. Kane, I. Peer, A. Darvasi, and T. Lencz. Implications for health and disease in the genetic signature of the Ashkenazi Jewish population. *Genome Biol.*, 13:R2, 2012.
 - [52] D. H. Alexander, J. Novembre, and K. Lange. Fast model-based estimation of ancestry in unrelated individuals. *Genome Res.*, 19:1655–1664, 2009.
 - [53] B. L. Browning and S. R. Browning. A unified approach to genotype imputation and haplotype-phase inference for large data sets of trios and unrelated individuals. *Am. J. Hum. Genet.*, 84:210–223, 2009.
 - [54] N. Patterson, A. L. Price, and D. Reich. Population structure and eigenanalysis. *PLoS Genet.*, 2:e190, 2006.